JGR Oceans

RESEARCH ARTICLE

10.1029/2024JC021120

Coherent Modes of Global Coastal Sea Level Variability

J. Oelsmann[1], F. M. Calafat[2], M. Passaro[1], C. Hughes[3], K. Richter[4], C. Piecuch[5], A. Wise[6], C. Katsman[7], D. Dettmering[1], F. Seitz[1], and S. Jevrejeva[6]

[1]Deutsches Geodätisches Forschungsinstitut (DGFI-TUM), Technical University of Munich, Munich, Germany, [2]University of the Balearic Islands, Palma, Spain, [3]University of Liverpool, Liverpool, UK, [4]NORCE Norwegian Research Centre AS, Bergen, Norway, [5]Woods Hole Oceanographic Institution, Woods Hole, MA, USA, [6]National Oceanography Centre, Liverpool, UK, [7]Delft Technical University, Delft, The Netherlands

Abstract Sea level variations in the coastal zone can differ significantly from those in the open ocean and can be highly spatiotemporally coherent in the alongshore direction. Yet, where and how coastal sea levels exhibit variations that emerge as persistent and recurrent patterns along the world's coastlines remain poorly understood. Here, we use a Bayesian mixture model to identify large-scale patterns of coherent modes of monthly coastal sea level variations from coastal altimetry and tide gauge data. We determine nine clusters of coherent coastal sea level variability that explain a majority of the monthly variance measured by tide gauges (1993–2020). The analysis of along track altimetry data enables us to detect several additional clusters in ungauged regions, such as the Indian Ocean or around the South Atlantic basin, which have so far been poorly described. Although some clusters (e.g., at the eastern boundary of the Pacific, the western tropical Pacific, and the marginal and semi-enclosed seas) are highly correlated with climate modes, other clusters share very little variability with the considered climate modes at the monthly timescale. Knowledge of these coherent regions thus motivates and enables further investigations on the impacts of local and remote forcing on coastal sea level variability, and the extent to which coastal sea level variability is decoupled from the adjacent deep ocean.

Plain Language Summary Coastal sea level variability can differ substantially from variability in the open ocean. This decoupling is mainly due to the presence of the continental slope, shallow waters, and coastlines. Coastal sea level variations are often highly coherent over the continental shelf, indicating the existence of persistent and recurrent spatiotemporal variations along the world's coastlines. However, the geographical distribution of these "coherent modes" has not been objectively investigated on a global scale, as previous studies have often relied on either sparsely distributed tide gauges or gridded altimetry and have not yet incorporated global and dedicated coastal altimetry products. Therefore, we use a Bayesian mixture model to identify large-scale patterns of coherent modes of monthly coastal sea level variations and complement the sparse tide gauge data with coastal altimetry. We show that much of the observed variability can be described by a relatively small number of cluster time series and thus be attributed to a set of common drivers. This knowledge of the predominant modes of variability is essential for future investigations aimed at better understanding the underlying drivers, the (de-)coupling of coastal and open ocean variability, and the associated implications for estimates of past and future coastal sea level variability.

Key Points:

- Using a Bayesian Mixture Model, we identify clusters of coherent coastal sea level variability from tide gauges and coastal altimetry
- Much of the global monthly coastal sea level variability can be described by a small set of clusters, suggesting common underlying drivers
- Regionally dependent links between climate modes and coastal sea level modes provide a basis for future analyses of the underlying drivers

Supporting Information:

Supporting Information may be found in the online version of this article.

Correspondence to:

J. Oelsmann,
julius.oelsmann@tum.de

Citation:

Oelsmann, J., Calafat, F. M., Passaro, M., Hughes, C., Richter, K., Piecuch, C., et al. (2024). Coherent modes of global coastal sea level variability. *Journal of Geophysical Research: Oceans*, *129*, e2024JC021120. https://doi.org/10.1029/2024JC021120

Received 15 MAR 2024
Accepted 27 OCT 2024

Author Contributions:

Conceptualization: J. Oelsmann, F. M. Calafat, M. Passaro, C. Hughes, K. Richter, C. Piecuch, A. Wise, C. Katsman, D. Dettmering, S. Jevrejeva
Data curation: J. Oelsmann, F. M. Calafat
Formal analysis: J. Oelsmann, F. M. Calafat, M. Passaro, C. Hughes, K. Richter, C. Piecuch, A. Wise, C. Katsman, D. Dettmering, F. Seitz, S. Jevrejeva
Funding acquisition: F. M. Calafat, M. Passaro, F. Seitz, S. Jevrejeva
Investigation: J. Oelsmann, F. M. Calafat, M. Passaro, C. Hughes, K. Richter, C. Piecuch, A. Wise, C. Katsman, S. Jevrejeva

1. Introduction

Sea level varies over a wide range of spatiotemporal scales reflecting the superposition of large-scale processes such as ocean mass changes due to land-ice melt, global mean thermosteric changes induced by global ocean temperature variations, and changes in the ocean circulation (Frederikse et al., 2019, 2020; Gregory et al., 2019; Hay et al., 2015; C. W. Hughes et al., 2018). In the open ocean, a large fraction of interannual to decadal sea level variability is linked to climate modes, with distinct sea level spatiotemporal structures in the global oceans (Han et al., 2017; Stammer et al., 2013; J. Wang et al., 2021). However, at the coast, sea level variability can differ substantially from variability in the open ocean and can be associated with different spatiotemporal characteristics (e.g., C. W. Hughes & Williams, 2010, C. W. Hughes et al., 2018). Such decoupling is due to the presence of the continental slope, shallow waters, and lateral boundaries (i.e., the coastlines), which mediate the transmission of open-ocean signals to the coast and give rise to a variety of coastal processes with short across-shelf length scales (Calafat et al., 2018; Cazenave et al., 2022; C. W. Hughes et al., 2018; C. Hughes et al., 2019; Woodworth et al., 2019).

Methodology: J. Oelsmann, F. M. Calafat, M. Passaro, C. Hughes, K. Richter, C. Piecuch, A. Wise, C. Katsman, D. Dettmering, S. Jevrejeva
Project administration: F. M. Calafat, F. Seitz, S. Jevrejeva
Resources: F. M. Calafat, D. Dettmering, F. Seitz, S. Jevrejeva
Software: J. Oelsmann, F. M. Calafat
Supervision: F. M. Calafat, M. Passaro, S. Jevrejeva
Validation: J. Oelsmann, F. M. Calafat
Visualization: J. Oelsmann
Writing – original draft: J. Oelsmann, F. M. Calafat
Writing – review & editing: J. Oelsmann, F. M. Calafat, M. Passaro, C. Hughes, K. Richter, C. Piecuch, A. Wise, C. Katsman, D. Dettmering, F. Seitz, S. Jevrejeva

Although coastal sea level variations can be decoupled from open-ocean variability, they are often highly coherent over the continental shelf, as evidenced by highly correlated signals up to several thousands of kilometers along the shore in observations from tide gauges, satellite altimetry, and ocean models (Calafat et al., 2013, 2018; Enfield & Allen, 1980, Hermann et al., 2009; Hogarth et al., 2020; C. Hughes & Meredith, 2006; C. Hughes et al., 2019; P. R. Thompson & Merrifield, 2014; P. R. Thompson et al., 2014). Coherent clusters of sea level variability can be found in many different regions of the world, such as along the northeast (NE) US coast, at the coasts of Western Europe, or Western Australia as illustrated by the highly correlated monthly tide gauge observations in Figure 1 (see also Papadopoulos and Tsimplis (2006)).

It is widely recognized that this alongshore coherence in sea level is largely established by the communication of signals along the coast by coastally trapped waves, which propagate cyclonically around the ocean basins on the continental shelf (i.e., away from the equator at the eastern boundary and toward the equator along the western boundary (C. Hughes et al., 2019)). Based on data from 60 tide gauge stations, Enfield and Allen (1980) identified alongshore wind-driven and poleward propagating signals, causing coherent sea level variations over up to 12,000 km along the eastern boundary of the Pacific. Longshore wind variations and the induced coastal wave propagation were also argued to permit highly coherent sea level variations along the eastern boundary of the North Atlantic and the Norwegian Sea (Calafat et al., 2012, 2013), which was also supported by subsequent studies (Chafik et al., 2019; Frederikse, Riva, Kleinherenbrink, et al., 2016; Frederikse, Riva, Slobbe, et al., 2016; Hermans et al., 2020; Hogarth et al., 2020). Several other studies have reported high coherence in sea level variations along the NE-US coast (see also Figure 1a) in observational and numerical studies, discussing possible influences of local wind or remote buoyancy forcing (Andres et al., 2013; Frederikse et al., 2017; Little et al., 2021; Piecuch et al., 2016; K. R. Thompson, 1986; O. Wang et al., 2022).

Because numerous other regions of coherent sea level variability have been identified (Calafat et al., 2018; Papadopoulos & Tsimplis, 2006; Piecuch, 2023; Steinberg et al., 2024), there are indications that coastal sea level exhibits variations that emerge as persistent and recurrent patterns along the world's coastlines. However, previous approaches aimed at identifying such clusters were either based on often manually selected groups of regionally distributed tide gauges (Dangendorf et al., 2021; Little et al., 2021; Papadopoulos & Tsimplis, 2006; Piecuch et al., 2016) or gridded altimetry (Camargo et al., 2023; P. R. Thompson & Merrifield, 2014) and have not yet included global and dedicated coastal altimetry products. Therefore, the geographic distribution of these "coherent modes," manifested as spatiotemporal clusters of coastal sea level variability, the degree of intra- and intercluster similarity, and the sensitivity to the timescale (i.e., monthly, annual, or interannual time scales) has not been objectively investigated on a global scale.

Robust identification and characterization of these clusters can help to understand whether sea level variability within a larger coastal region can potentially be linked to a set of common drivers and whether these are related to large-scale climate variability or have different origins. This knowledge can also play a key role in current efforts to understand the extent to which changes in the open ocean affect coastal sea level (Calafat et al., 2013; Cazenave et al., 2022; Intergovernmental Panel on Climate Change (IPCC), 2023; Little et al., 2021; Steinberg et al., 2024; Woodworth et al., 2019) and thus also enable a better understanding of past global mean sea level changes. This is because historic changes are often reconstructed by identifying groups of highly correlated tide gauges or by reconstructing open ocean variations (often represented by empirical orthogonal functions (EOFs)) from coastal tide gauge observations (Church & White, 2011; Dangendorf et al., 2019; Frederikse et al., 2020; Jevrejeva et al., 2006; P. R. Thompson & Merrifield, 2014). Finally, a better understanding of the drivers and spatiotemporal scales of these modes can also support the assessment of future coastal sea level changes and their uncertainties in projections.

A major obstacle to the characterization of coastal sea level changes is the inhomogeneous global coverage of tide gauges, which has hampered analyses in many regions, such as South America, Africa, or Asia. These observational gaps are now being closed due to the steady improvement of altimetry data near the coast (Cazenave et al., 2022). Due to steady improvements in the retracking of coastal altimetry data as well as coastal adjustments and corrections over the last decades (Cazenave et al., 2022; Fernandes & Lázaro, 2016; Passaro et al., 2014), we are now able to complement the partially sparse tide gauge network and resolve coastal sea level dynamics on a global scale. The inclusion of the more uniformly distributed altimetry data (as opposed to the heterogeneously distributed tide gauge data) is also important for the interpretation of certain clusters when they are mainly detected due to a high local density of tide gauges. Here, we provide a systematic global assessment of coastal sea

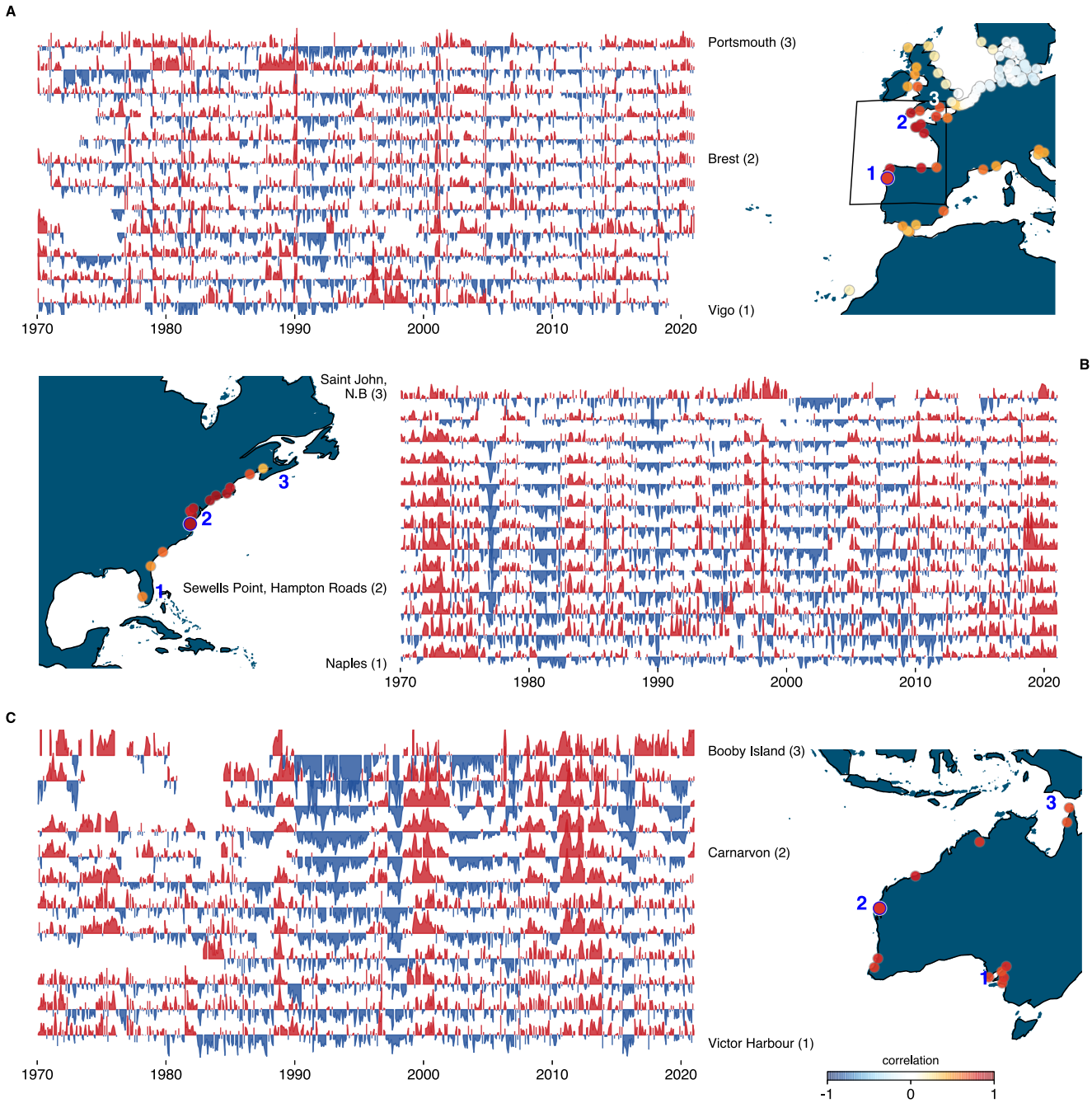

Figure 1. Time series of monthly detrended and deseasoned sea level anomaly observations from tide gauges on the (a) southwestern European coast, (b) the northeast US coast, and (c) western Australia. The maps show the correlation between all-time series and an average of all tide gauge time series except for the map in (a), where the correlations are computed with an average of all tide gauge time series between Malaga and Portsmouth. The numbers link the time series to the tide gauges shown on the map.

level variability by extending the tide gauge network with coastal satellite altimetry. We seek to determine if where and how coastal sea levels exhibit variations, which emerge as persistent and recurrent pattern along the world's coastlines. Further, we investigate whether coastal sea level, similar to climate modes, exhibits spatially stationary modes of variation. We address the following research questions:

⇒ Over what regions are coastal sea level variations spatially coherent and do the geometries of these regions vary as a function of time?

Table 1
Applied Models and Geophysical Corrections for Estimating Sea Surface Heights

Parameter	Model/Method	Reference
Range and Sea State Bias	ALES	Passaro et al. (2014, 2018)
Inverse barometer	DAC-ERA[a], DAC	Carrère et al. (2016), Carrère and Lyard (2003)
Wet troposphere	GPD+[a], VMF3	Fernandes and Lázaro (2016), Landskron and Böhm (2018a, 2018b)
Dry troposphere	VMF3	Landskron and Böhm (2018a, 2018b)
Ionosphere	NIC09	Scharroo and Smith (2010)
Ocean and Load tide	FES2014	Carrèreet al. (2015)
Solid Earth and Pole tide	IERS 2010	Petit and Luzum (2010)
Mean Sea surface	DTU18MSS	Andersen et al. (2018)
Radial errors	MMXO	Bosch et al. (2014)

[a]If available.

⇒ Does the more complete and spatially homogeneous coverage of altimetry permit the identification of clusters, which are not apparent in the tide gauge data?

⇒ To what extent are these regions of coherent sea level variations related to large-scale climate modes on monthly time scales?

Previous approaches to determine clusters of coherent sea level variations often involved, for example, the analysis of sorted cross-correlation matrices (Calafat et al., 2018; Dangendorf et al., 2021; Little et al., 2021; Piecuch et al., 2016), agglomerative hierarchical cluster analysis (P. R. Thompson & Merrifield, 2014), EOFs (Papadopoulos & Tsimplis, 2006), or self-organizing maps (Camargo et al., 2023; Hardman-Mountford et al., 2003; Liu et al., 2016). In this study, we use Bayesian mixture models (see Section 2.3) to probabilistically infer the cluster membership of globally distributed monthly tide gauge and altimetry observations. This approach has advantages over the correlation-based (or the EOF) approach in that it provides a rigorous uncertainty quantification of the estimated components (cluster time series) and allows the incorporation of several model properties. These include cluster time series properties (i.e., the implementation of autocorrelated processes) as well as cluster-dependent noise amplitudes, that is, of the variations of the observations around a cluster mean time series. Furthermore, the detected modes do not necessarily have to be orthogonal to each other (as in the EOF analysis). As opposed to EOF analysis, where the linear combination of a set of functions explains the variance of a data set, the Bayesian mixture model is used to identify a set of time series, where each time series best represents the variability of a cluster of stations (e.g., the tide gauges). This is particularly useful for identifying regionally separated clusters.

In Sections 3.1, 3.2, and 3.3, we investigate the global pattern of coherent modes of coastal sea level variability using tide gauges and coastal altimetry. We show that a large fraction of the coastal sea level variability can be described by a relatively small set of time series, which supports the existence of common modes along the world's coastline. In Section 3.4, we investigate the influence of timescale on the detected clusters. We explore how these coastal modes relate to large-scale climate modes in Section 3.5.

2. Data and Methods

2.1. Sea Level Observations From Altimetry and Tide Gauge Data

To provide observations at coastlines, where no tide gauge data are available, we use dedicated coastal 1-Hz along-track altimetry data of the missions Jason 1–Jason 3 from Schwatke et al. (2023). The data cover a period of 20 years (January 2002–December 2021). All satellite orbits are referenced to the ITRF2014 reference frame (Altamimi et al., 2016). To compute the sea surface heights (SSHs) and sea level anomalies (SLAs), we apply the range adjustments and corrections as listed in Table 1.

The systematic differences between the different missions are reduced by the global multi-mission crossover analysis (MMXO) (Bosch et al., 2014; Bosch & Savcenko, 2007). To compute the SSH time series, we map the

altimetry records on the 1-Hz nominal tracks consistent with the CTOH nominal paths (Center for Topographic studies of the Ocean and Hydrosphere, www.ctoh.legos.obs-mip.fr) with nearest neighbor interpolation. We also apply an outlier check to reject extreme values in the along track data. Outliers are detected if (a) the SSH values are greater than 2 m (after subtracting the mean sea surface), (b) the absolute difference of the data and its running median (centered, over 20 points along the track) is greater than 12 cm, and if (c) the difference of consecutive points (along the track) exceeds 8 cm (see also Oelsmann et al. (2021)). Because we compare the data with monthly tide gauge (TG) observations, we compute monthly averages of the SSH data (with an original temporal resolution of 10 days).

To estimate clusters of coastal sea level variability from the altimetry observations, we create a time series at the intersections of the TOPEX/Poseidon nominal tracks with the coastline. At every track, we average the 1-Hz altimetry data within 15 km to the coast, resulting in a set of 1,497 virtual stations (similar to Cazenave et al. (2022)). Here, the chosen distance of 15 km represents a trade-off between being very close to the coast and ensuring the robustness of the coastal averages, as altimetry observations very close to the coast could lead to spurious signals in the coastal averaged time series. Although previous studies have examined signals much closer to the coast (i.e., in the last 3 km), we find evidence that the monthly variations are coherent on much larger spatial scales (in the across-shelf direction) as in more than 98% of the cases (virtual stations) the across-shelf correlation decay-scales are larger than 20 km.

Next to the altimetry data, we use 634 tide gauge time series (covering January 1993–December 2020) from PSMSL (Permanent Service for Mean Sea Level, https://www.psmsl.org/, Holgate et al. (2013)). The monthly data are adjusted for the inverse barometer effect based on sea-level pressure data from the NCEP/NCAR reanalysis (Kalnay et al., 1996). For the clustering and correlation analyses, we deseason, detrend, and demean the coastal altimetry and tide gauge data (i.e., the annual and semiannual signals and trends (over the full period) are estimated through ordinary least squares). Thus, for these analyses, we primarily focus on coherence on monthly timescales and exclude changes on longer timescales (contributions from vertical land motion, etc.).

2.2. Climate Mode Indices

The northern hemispheric climate indices (North Atlantic Oscillation (NAO), the East Atlantic Pattern (EA), the Pacific North American Pattern (PNA), the East Atlantic/West Russia Pattern (EA/WR), the Scandinavia Pattern (SCA)), are obtained from https://www.cpc.ncep.noaa.gov/data/teledoc/telecontents.shtml. The El Niño-Southern Oscillation (ENSO) index is obtained from https://psl.noaa.gov/enso/mei/data/meiv2.data, the Arctic Oscillation (AO) from https://www.cpc.ncep.noaa.gov/products/precip/CWlink/daily_ao_index/ao.shtml, the Pacific Decadal Oscillation (PDO) index from https://www.ncei.noaa.gov/pub/data/cmb/ersst/v5/index/ersst.v5.pdo.dat, the Indian Ocean Dipole (IOD) from https://psl.noaa.gov/gcos_wgsp/Timeseries/Data/dmi.had.long.data. We use the climate indices ENSO, NAO, AO, PDO, PNA, and IOD, because they are among the most prominent modes in the different basins and have been previously analyzed in the context of coastal sea level variability (Han et al., 2019; Royston et al., 2022; J. Wang et al., 2021) and also include EA, EA/WR, and SCA. All climate mode time series are detrended and deseasoned as the other tide gauge and altimetry data.

2.3. Bayesian Gaussian Mixture Models

We use a Gaussian mixture model to cluster the tide gauge stations into groups of coherent variability (e.g., Mclachlan & Basford, 1988; McLachlan & Peel, 2000). The same model is used to cluster the virtual stations from altimetry; hence in the following, when we refer to tide gauge stations, this also applies to virtual stations. To lay the basis for the formulation of the mixture model, we start by assuming that any given tide gauge record can be drawn from one of K normal distributions, each one with its own location $\mu_{t,k}$ and scale σ_k, for $k = 1, \cdots, K$ and $t = 1, \cdots, T$, where T is the number of months spanned by the tide gauge observations. In other terms, we assume that there are K regions or clusters of coherent sea level variability, and each tide gauge record belongs to one of such regions. The locations $\mu_{t,k}$ are the latent time series of coherent sea level variability in each cluster (unknown and to be estimated), whereas the scales σ_k are a measure of the amount of variation with respect to $\mu_{t,k}$ across tide gauge records in each cluster due to small-scale variability and observational errors (also unknown and to be estimated). The number of clusters K needs to be specified a priori. We test a different number of clusters as explained later in this section.

The way to implement such a model is to express the likelihood as a mixture of normal distributions. Mixture models are typically parameterized in terms of a categorical variable $z_n \in 1, \cdots, K$ for $n = 1, \cdots, N$, where N is the total number of tide gauges stations. The assignment z_n indicates which cluster (i.e., mixture component) the n-th tide gauge station belongs to and it is distributed according to a categorical distribution:

$$z_n \sim categorical(\mathbf{p}) \tag{1}$$

where $\mathbf{p} = (p_1, \cdots, p_K)$ is a vector of event probabilities with $p_k > 0$ and $\sum_{k=1}^{K} p_k = 1$. The quantity p_k indicates the probability with which the k-th mixture component occurs, and thus we will refer to the p_k's as the mixture proportions. If we now let $Y_{t,n}$ be the sea level at month t as measured by the n-th tide gauge, then the mixture likelihood is:

$$Y_{t,n} \sim normal\left(\mu_{t,z_n}, \sigma_{z_n}^2\right) \tag{2}$$

In practice, the discrete parameters z_n are challenging to estimate. Hence, to facilitate inference, we marginalize these parameters out. After this marginalization, the mixture likelihood can be written as a linear combination of the mixture components:

$$Y_{t,n} = \sum_{k=1}^{K} p_k \left(\mu_{t,k} + e_{t,k}\right) \tag{3}$$

where $e_{t,k}$ are assumed to be i.i.d. (independent and identically distributed) normal random variables $e_{t,k} \overset{\text{iid}}{\sim} normal\left(0, \sigma_k^2\right)$. Note that, because $p_k > 0$ and $\sum_{k=1}^{K} p_k = 1$, the linear combination expressed by Equation 3 is, in fact, a convex combination.

Here, we adopt a Bayesian approach to inference, which means that the mixture likelihood needs to be supplemented with a prior distribution to form the posterior distribution, as explained in the following. The model is specified as a Bayesian hierarchical model with three levels: (a) a probability model that describes the distribution of the sea-level observations conditional on the latent process $\mu_{t,k}$ and some parameters (data model); (b) a probability model that describes the temporal evolution of $\mu_{t,k}$ conditional on a set of parameters (process model); and (c) a prior distribution that describes the prior belief about the model parameters. Inferences are made by drawing samples from the posterior distribution of the processes and parameters given the observations, which is proportional to the product of the three probability models outlined above. Next, we describe the three levels of the hierarchical model.

The data model is given by Equation 3. In the process model, the locations of the mixture normal distributions, $\mu_{t,k}$, are assumed to follow a second-order autoregressive process (AR2):

$$\mu_{t,k} = \phi_{1,k}\mu_{t-1,k} + \phi_{2,k}\mu_{t-2,k} + v_{t,k} \tag{4}$$

where $\phi_{1,k}$ and $\phi_{2,k}$ are autoregressive coefficients and $v_{t,k}$ are i.i.d. normal random variables $v_{t,k} \overset{\text{iid}}{\sim} \mathcal{N}\left(0, \tau_k^2\right)$, where τ_k is a scale parameter (to be estimated) that effectively controls the magnitude of the variability of the time series in each cluster. The initial values $\mu_{0,k}$ are modeled in the parameter layer of the Bayesian mixture model by placing a prior distribution on them. Note that, although more complex time series models could be used, we use here the AR2 model, because it describes the data sufficiently well (see Section 3.1).

Finally, the parameter layer contains six unknown parameters (p_k, $\phi_{1,k}$, $\phi_{2,k}$, σ_k, τ_k, and $\mu_{0,k}$) on which we place the following prior distributions. The mixing proportions are constrained to the unit simplex (i.e., $p_k \geq 0$ and $\sum_{k=1}^{K} p_k = 1$) as they are probabilities and thus they are assigned a Dirichlet distribution: $p_k \sim Dirichlet(K)$. The scale parameters σ_k and τ_k are given half-normal distributions (units in meters): $\sigma_k \sim half - normal(0, 1.5)$ and $\tau_k \sim half - normal(0, 1.5)$. For the initial state of the AR2 process, we assume a normal distribution: $\mu_{0,k} \sim normal(0, 3)$. Finally, in assigning priors to the autoregressive coefficients, we should enforce the following stationarity conditions: $\phi_{2,k} < 1$ and $\phi_{2,k} - 1 < \phi_{1,k} < 1 - \phi_{2,k} < 1$. In addition to these conditions, it is important to note that, because the component distributions of the mixture model are identical (i.e., they are all

normal distributions), it is not possible to distinguish which parameters of the model are associated with each mixture component. To break this label degeneracy, we introduce an intermediate parameter $\phi_i \sim Dirichlet(K+1)$ and then assume that $\phi_{2,k} = 2\sum_{i=1}^{K}\phi_i - 1$. This formulation ensures that $|\phi_{2,k}| < 1$ and, at the same time, breaks the label degeneracy by forcing the $\phi_{2,k}$ to be ordered. For the other autoregressive coefficient, we assume a uniform distribution: $\phi_{1,k} \sim uniform\left(\phi_{2,k} - 1, 1 - \phi_{2,k}\right)$.

The posterior probability Pr that the tide gauge TG_n belongs to the mixture component k can be computed as

$$\Pr(\mathrm{TG}_n \in k) = \frac{p_k normal\left(\mathbf{Y}_n | \boldsymbol{\mu}_k, \sigma_k^2\right)}{A} \tag{5}$$

where $\mathbf{Y}_n = (Y_{1,n}, \ldots, Y_{T,n})$, $\boldsymbol{\mu}_k = \left(\mu_{1,k}, \ldots, \mu_{T,k}\right)$, and A is a normalization constant that can be computed by summing over all of the K mixture components. Membership for each tide gauge station is assigned to the cluster that gives the maximum posterior probability.

The Bayesian mixture model is fitted using the No-U-Turn Sampler (NUTS) as implemented by the Numpyro probabilistic programming language (Phan et al., 2019). We run NUTS with four chains of 1,250 iterations each (warm-up = 1,000) for a total of 5,000 post-warm-up draws.

We determine clusters of coherent sea level variations based on monthly tide gauge observations and coastal altimetry data using the Gaussian mixture model (described in Section 2.3). Prior to this analysis and in order to define an optimal number of clusters used for each data set, we iteratively estimate different numbers of clusters for the altimetry ($K = 3, \ldots, 34$) and tide gauge data set ($K = 1, \ldots, 20$, see Figure S1 in Supporting Information S1). Based on the dependency between the average variance explained and different numbers of clusters K, we select the optimal number of clusters at a threshold where increasing the number of clusters does not substantially improve the explained variance anymore (an approach also referred to as the "elbow method" (Thorndike, 1953)). Accordingly, we use 20 clusters for the tide gauge data and for the altimetry data set. We sort the different cluster labels k such that the altimetry and tide gauge clusters are comparable. Note that although the number of clusters selected is still somewhat subjective and may differ when determined by other methods, we do not expect substantial differences for other numbers, as we have found largely consistent geographic distributions of clusters, for example, for the tide gauge data set for $K = 12, \ldots, 20$ (see also Figure S1 in Supporting Information S1).

3. Results

3.1. Regional Cluster of Coherent Sea Level Variations

The geographical distribution of the different detected clusters (based on monthly data) are shown in Figures 2a and 2b and selected cluster time series (i.e., the posterior means) are provided in Figure 4. Both, the tide gauge clusters and the altimetry-based clusters form regionally confined groups. This underlines the inherent regional coherence of coastal sea level, as such a regional confinement is not enforced within the model itself (distances between stations are unknown to the model). Overall, there is a high correlation between the estimated tide gauge cluster time series $\mu_{t,k}$ and most of the tide gauge time series within the respective clusters (Figures 2c and 4b). There are nine tide gauge (Figure 4) clusters that show an average correlation of 0.82 (i.e., the average of the averaged correlations between the cluster time series and the associated tide gauge time series). The corresponding altimetry-based clusters have a lower correlation of 0.6. Note that we discuss differences between the data sets and poorly correlated clusters in more detail in Section 3.2.

We identify seven clusters, where the altimetry-based clusters coincide with those derived from tide gauge observations and have a correlation of at least 0.5 with each other (as shown in Figure 3). These detected clusters indicate the major regions of coherent sea level variations and include the NW-US coast (e.g., Enfield & Allen, 1980; Han et al., 2019; Woodworth et al., 2019), the Gulf of Mexico (including parts of the SE-US coast up to Cape Hatteras, or the Oregon Inlet Marina tide gauge) (Rashid et al., 2019; P. R. Thompson & Mitchum, 2014), the North Sea (including the tide gauges along the Norwegian Coast (e.g., Calafat et al., 2012, 2013; Chafik et al., 2019; Frederikse, Riva, Kleinherenbrink, et al., 2016; Frederikse, Riva, Slobbe, et al., 2016; Hermans et al., 2020; Hogarth et al., 2020; C. Hughes & Meredith, 2006)), the Baltic Sea (e.g., Grawe et al., 2019; Hünicke

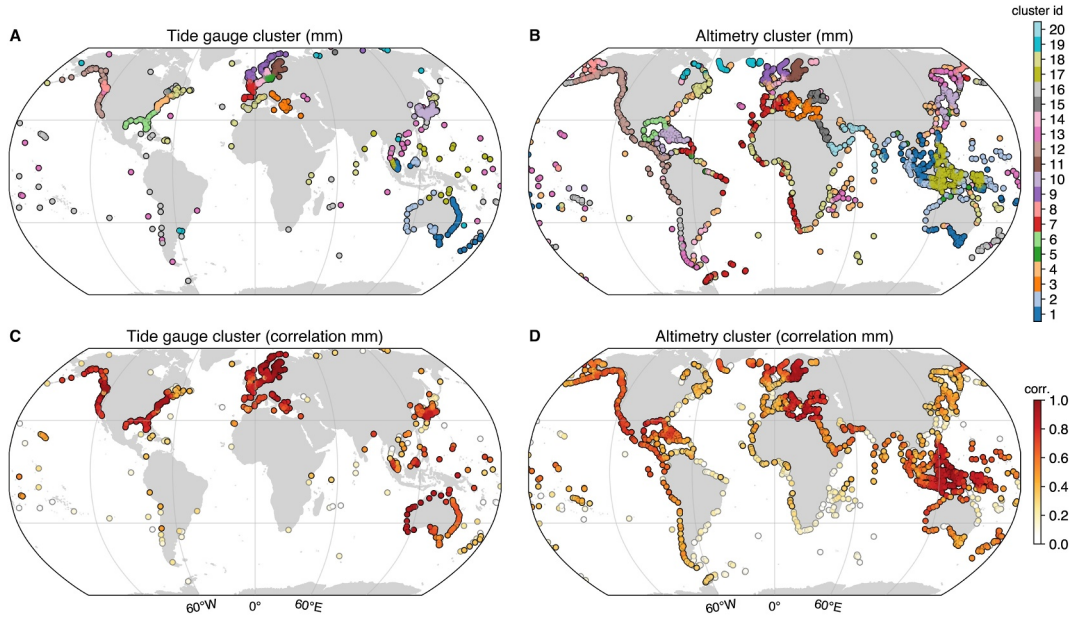

Figure 2. Clusters based on monthly mean (mm) tide gauge (a) and coastal altimetry (b) observations, as derived by the Bayesian mixture model approach described in Section 2.3. (c) and (d) Show correlations of cluster time series $\mu_{t,k}$ with the associated monthly individual (virtual) station time series. Points with correlations below 0.3 are shown as gray-outlined circles.

& Zorita, 2006; Passaro et al., 2021), the eastern Mediterranean Sea, the Western Australian Coast and parts of the South China Sea as well as the Sea of Japan. The uncertainties of the cluster mean time series, which are here computed as the temporally averaged standard deviation across the samples $\mu_{k,t}$ of the from the posterior distribution, provide an estimate of the uncertainty around the cluster mean required to account for the spread of observations associated with the cluster. As the cluster mean uncertainty is usually in the order of 0.5 cm for the aforementioned clusters, it supports the robustness of the detected clusters. In Figure 4c, we show the scaled uncertainties derived as the temporally averaged standard deviation across the samples $\mu_{k,t}$ of the posterior distribution divided by the temporal standard deviation of the cluster mean time series. This shows that the uncertainties of the cluster mean time series for these most robust clusters are usually below 20% of the absolute variability of the cluster mean time series. These uncertainties are approximately inversely proportional to the correlations of the cluster mean time series with the individual stations. As can be seen in Figure 4b, the correlations for the aforementioned clusters are usually larger than 0.7. Correlations for the altimetry-based clusters are only slightly but systematically smaller than the tide-gauge-based clusters. This is, on the one hand, expected due to the remaining inaccuracies in the coastal altimetry data from measurement, correction, or geophysical adjustment errors but, on the other hand, also supports the substantial improvements in accuracy over the last decade (Passaro et al., 2014; Cazenave et al., 2022), as differences in the correlations between the data sets are usually small (for the most robust clusters).

To better emphasize the boundaries between the individual clusters, we show in Figure 5 the correlations of each cluster time series with the globally distributed tide gauges (empty circles) or coastal altimetry intersections (small outlined circles), which are spatially sorted along the coastlines starting from the Gulf of Alaska. For each cluster and data type, we added bars to indicate where four consecutive data points have a correlation greater than 0.4 within the cluster time series in order to better separate the clusters from each other. This representation of the regional distribution of the clusters demonstrates that, indeed, a large fraction of the global coastal sea level variations can be divided into individual clusters. Some of these clusters are also (anti) correlated with others, for example, the northern Europe and the Baltic Sea level variations are highly correlated (Frederikse, Riva, Kleinherenbrink, et al., 2016; Passaro et al., 2021), whereas the NW-US cluster and the Western Australian/South China Sea cluster are slightly anticorrelated.

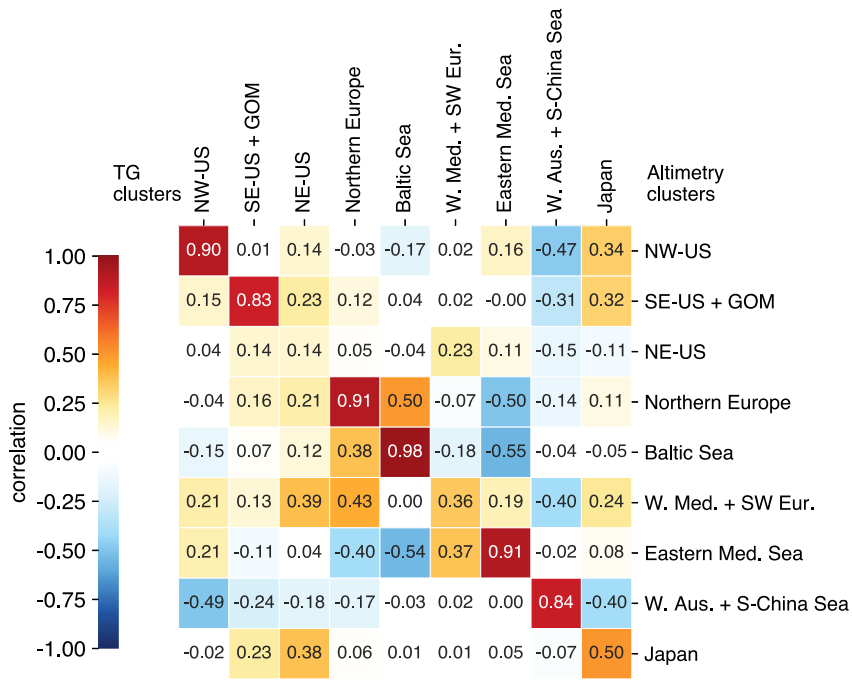

Figure 3. Correlations between the cluster mean time series of the tide gauge (columns) and the altimetry (rows) data.

3.2. Differences Between Altimetry and Tide Gauge Clusters

Although the altimetry and tide gauge clusters often agree qualitatively, some of them differ in their regional extent and in how well they represent the underlying individual time series data (as indicated by the correlation with the cluster time series in Figures 2c, 2d, and 4b and by the scaled uncertainty in 4C). Such poorly correlated station time series are represented by the gray outlined circles (Figures 2a and 2b), which (for the altimetry data set) are more abundant at the western boundaries of the ocean, that is, at the eastern coasts of South America, Africa, Australia, or North America (i.e., the NE-US coast cluster). We also note that in some cases, even though the clusters are indicated by the same color, they may not overlap perfectly for the different data sets, tide gauges, and altimetry.

Differences between the data sets are found for the Japanese cluster, the southwestern European/western Mediterranean cluster, at the NE-US coast, and, to some extent, for the NW-US coast. At the NE-US coast, the tide gauges are highly correlated with their respective cluster time series in contrast to the altimetry data (Figures 2a, 2b, and 4b, Figures S3B and S5B in Supporting Information S1). The tide-gauge-based cluster extends from north of Cape Hatteras from the Duck Pier Outside tide gauge to the Eastport tide gauge (e.g., Andres et al., 2013; Calafat et al., 2018; Little et al., 2021; Piecuch et al., 2016; K. R. Thompson, 1986; O. Wang et al., 2022). The differences between the detected clusters in the data sets may be caused by the data distribution or the accuracy of the altimetry data in the coastal zone. Since there are many more tide gauge stations in that region (compared to the virtual coastal altimetry stations), the NE-US cluster may be more easily detected by the Bayesian mixture model in the tide gauge data set, which is also reflected by higher correlations (Figure 2c). Since the Bayesian mixture model does not take into account the geographic distribution or density of the data, it treats all observations equally, which naturally leads to more robust estimated clusters in regions of high data density (see also Figure S3 in Supporting Information S1). In addition, the altimetry-based NE-US cluster appears to absorb very distant and randomly distributed data points, which essentially act as noise and drastically reduce the overall correlation of this cluster with the underlying data (Figure 5). Note, that similar difficulties with detecting a robust cluster at the NE-US coast also exist for alternative data sets (gridded altimetry) or different clustering approaches (hierarchical agglomerative clustering) as explained in Supporting Information S1 and by Figure S5 in Supporting Information S1. Thus, this case is likely caused by the data-distribution and not the nature of the clustering approach. Therefore, the combined consideration of altimetry and tide gauges is necessary for the interpretation of the detected clusters. This is mainly because the tide-gauge-based clusters and altimetry-based clusters represent

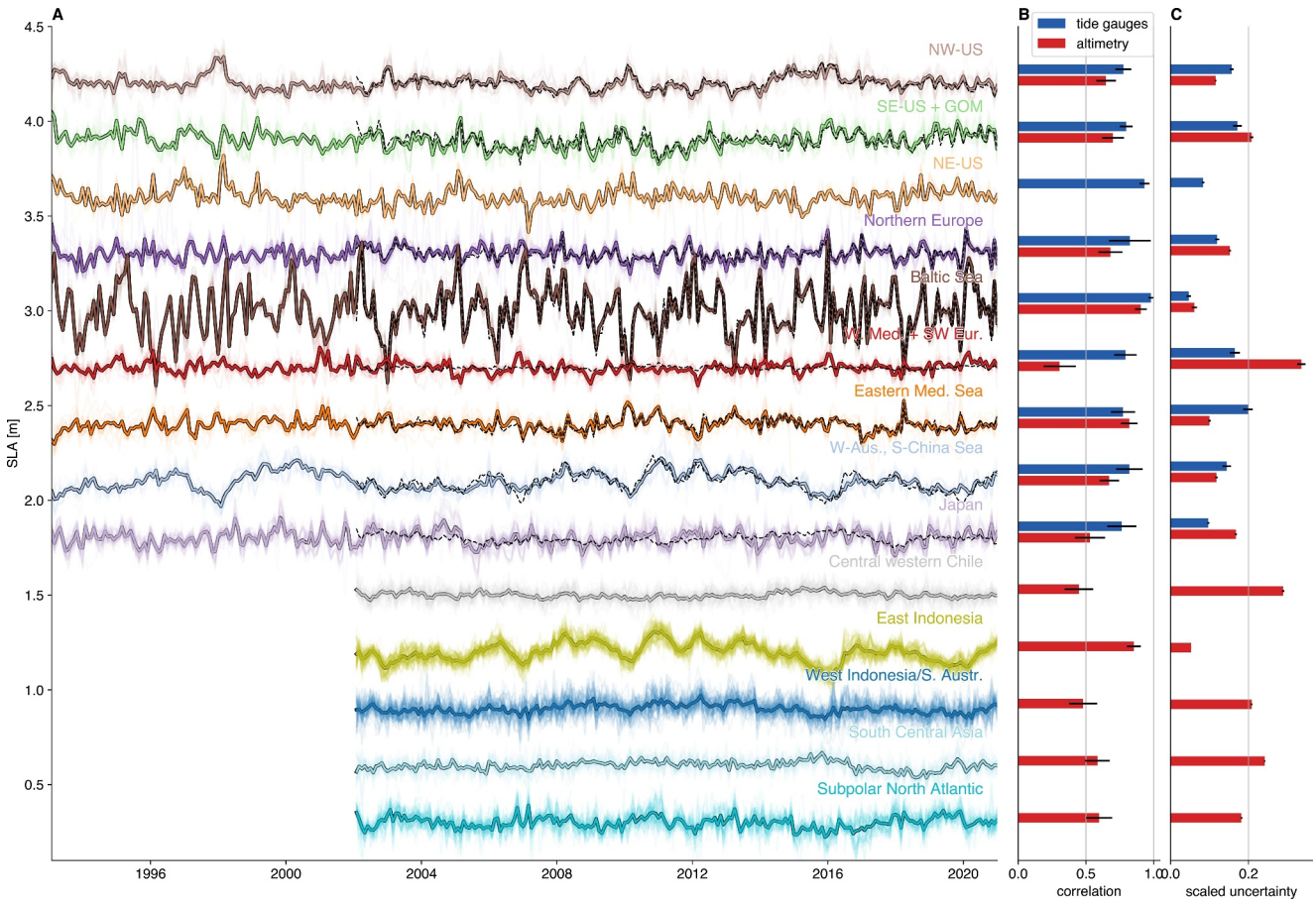

Figure 4. (a) Shows time series of 14 selected clusters (thick lines) based on tide gauges (until and including the Japan cluster) and on altimetry (after the Japan cluster). Above the Japan cluster the altimetry cluster time series are represented by dashed lines. The individual time series of the tide gauges and the altimetry data are illustrated by transparent lines. (b) Shows the average correlation of every cluster time series with all station time series associated with that cluster for tide gauges (blue) and altimetry (red). (c) Represents the temporally averaged scaled uncertainty of the cluster time series, that is, the temporally averaged standard deviation across every sample $\mu_{k,t}$ from the posterior distribution for the individual clusters divided by the temporal standard deviation of the cluster mean time series, in cm, for the tide gauge (blue) and altimetry (red) data.

two distinct experiments in terms of data distribution (notwithstanding their other differences): one more uniform and homogeneous (altimetry) and one more nonuniform and heterogeneous (tide gauge). The extent to which they produce analogous clusters gives us confidence that the clusters we identify are not simply artifacts of high-density sampling of local behavior by tide gauges.

Differences in the data distribution may also cause the NW-US coast cluster (in the tide gauge data set) to be interrupted by another cluster (shown here as cluster number eight in Figure 4a) starting from the Charleston 2 tide gauge (Oregon) until the Bella tide gauge (British Columbia). In this region, the tide gauge data set has a much denser coverage than the virtual stations from altimetry. Although this cluster is still highly correlated with the NW-US coast cluster (0.79), the standard deviation of the cluster mean time series (for cluster number 8) is increased (5.4 cm) compared to the NW-US coast cluster (3.8 cm) with increased variability at higher frequencies (i.e., the monthly timescale). The separation of the clusters may be explained by the increased relative importance of local longshore wind forcing and wind stress curl north of San Francisco, which superimpose remotely forced variations of equatorial origin that are dominant southward of San Francisco (Enfield & Allen, 1980; P. R. Thompson et al., 2014).

There also exist differences between the data sets (altimetry and tide gauges) for the southwestern European/western Mediterranean cluster (red colors in Figures 2, 4, and 5). In contrast to the altimetry data set, the southwestern European/western Mediterranean cluster is split up into two modes for the tide gauge data. The geographic extent of both tide gauge clusters largely coincides with the coherent sea level variations described in

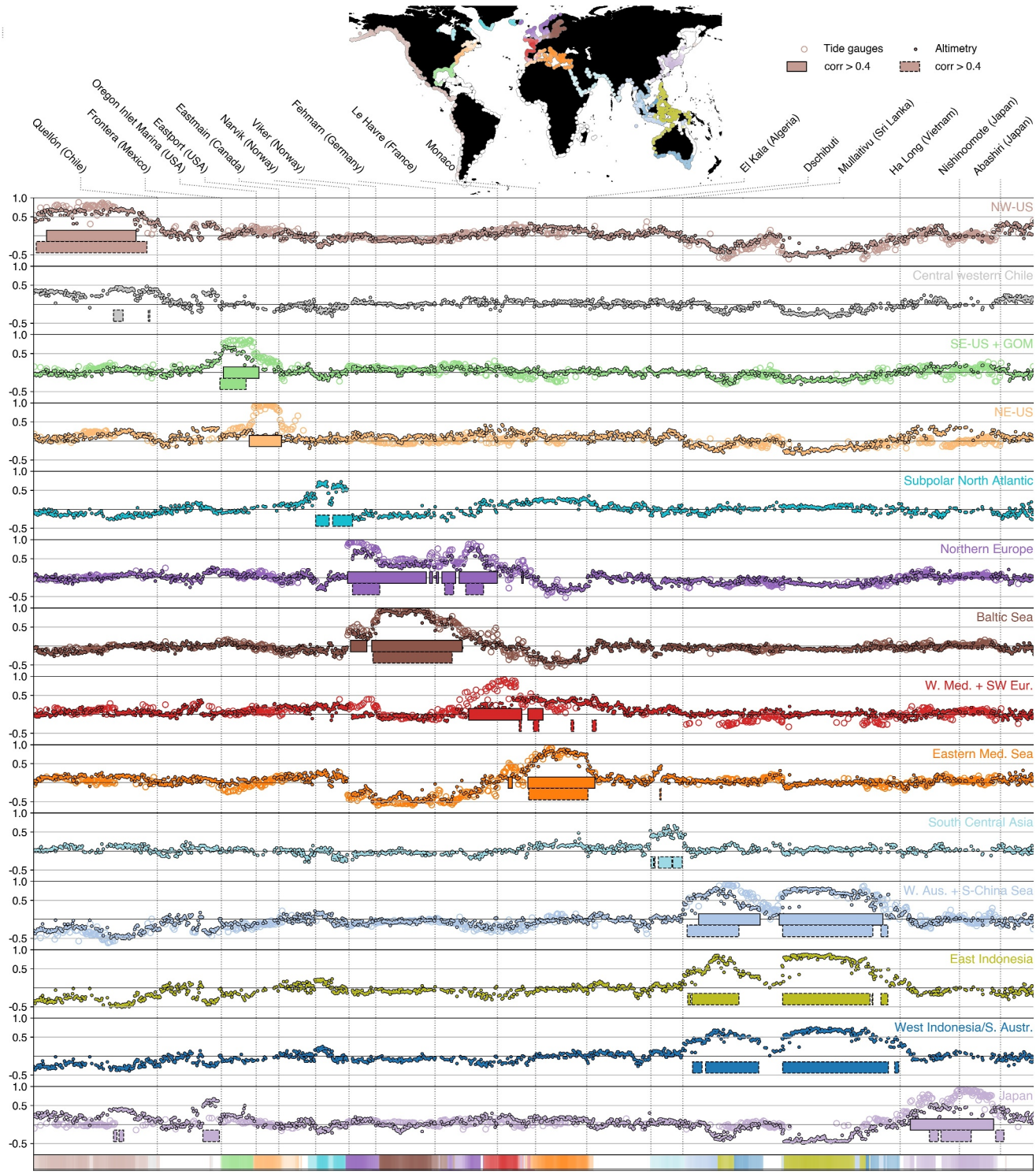

Figure 5. The individual rows show correlations of the cluster mean time series with the individual tide gauge (empty circles) or altimetry (small circles) time series at different locations. The stations are sorted along the coastal profile (starting from Alaska (left) to Russia (right)) as indicated by the colored contour in the map (and the color bar at the bottom) in which the opacity is scaled by the correlation of the individual time series with the cluster time series. The horizontal bars indicate where the rolling mean of four consecutive points have a correlation larger than 0.4.

earlier work (Calafat et al., 2012, 2013) that attributed longshore wind variations and the induced Kelvin waves propagation to increased coherence along the coast. Despite the regional overlap, the associated altimetry-based cluster (Figure 5) is less correlated with the individual time series and also contains more points along the East African coastline and the south Caribbean Sea (Figure 2b). Due to averaging across these observations, the temporal variability of the cluster mean time series is substantially reduced for the altimetry data compared to the tide gauge data (Figure 4). This is also reflected by the enhanced scaled uncertainties of that cluster (Figure 2). Still, since some of the tide gauges on the Canaries and in the Caribbean Sea are also connected to the western Mediterranean cluster (Figure 2a), there seems to be some shared variability across the western tropical and eastern extratropical Atlantic (which is partially present also in gridded altimetry data, Camargo et al. (2023)).

We have only moderate confidence in the cluster results for New Zealand. Although the tide-gauge results assign the coastal sea level variations around New Zealand to the western Indonesia/southern Australia cluster, the average correlation of all tide-gauge time series with the cluster mean time series is only 0.26. In contrast, for the altimetry data, New Zealand is in the same cluster as central western Chile. Although the average correlations of the virtual station with this cluster mean are higher (0.53) than those obtained for the tide gauge network, this explains only a small fraction of the total variance.

As there are sometimes ambiguities between the altimetry and tide-gauge-based clusters, we perform an additional cluster analysis on a merged altimetry and tide gauge data set (Figure S4 in Supporting Information S1). The resulting clusters are broadly consistent with both the altimetry and tide-gauge-based estimates (the Baltic Sea, the North Sea, the eastern Mediterranean Sea, and east Indonesia) and increase the confidence in these detected clusters. The merged data set also confirms the existence of coherent modes along the NE-US coast and the southwestern European/western Mediterranean coastlines, which is consistent with the tide gauge-based results and previous investigations (Andres et al., 2013; Calafat et al. (2012, 2013); Piecuch et al., 2016; K. R. Thompson, 1986). However, in other cases, such as for the NW-US coast and the Gulf of Mexico, the clusters are spatially separated from each other at locations where tide gauges are not available. Therefore, the interpretation of this merged data set with respect to the physical processes generating these clusters is sometimes hampered, as the results may be influenced by the varying availability and differences in accuracy of the data types. Hence, a separate analysis of both data types is necessary to understand the influence of data distribution on the regional extent of the clusters.

3.3. Filling Unobserved Gaps With Altimetry Data

A key limitation to our understanding of the global coherent regions of sea level variability is that many coastal regions are unobserved by the tide gauge network. The special value of filling observational gaps along the coast with altimetry is demonstrated in Figures 2b and 5. There are several regions where additional clusters can be detected, or where more information about the spatial extent of the clusters can be obtained with the coastal altimetry data set.

For example, the NW-US coast cluster extends much further south than observed by tide gauges alone (Figures 2b and 5). This is in line with several previous studies (Enfield & Allen, 1980; C. Hughes & Meredith, 2006), discussing a common equatorial origin to drive sea level variations along the western coast of North and South America. Other additionally identified coherent clusters are located, at the coasts of the Caribbean Sea, around Nantucket Island (O. Wang et al., 2022), eastern and western Indonesia, the Arabian Peninsula (South Central Asia, consistent with (Piecuch et al., 2021), in particular Figure 8), in the northernmost subpolar North Atlantic, and in the Red and Black Seas (Figures 2b, 4, and 5). Most of these clusters, similar to the tide gauges, show a high regional coherence and capture coastal sea level variability that is largely decoupled from the neighboring regions (i.e., the subpolar North Atlantic or the South Central Asia clusters, see Figure 5).

Also, the coastal regions around Southeast Asia are better resolved with the coastal altimetry data. This region is divided into three clusters: the western Australian/South China Sea cluster, the east Indonesia cluster, and the west Indonesia/southern Australia cluster (Figure 2b). Even though the cluster time series are highly correlated with each other (with a correlation of at least 0.79), they are geographically clearly separated. This is partially due to the differences in their amplitudes of variability, for example, the west Indonesia/south Australia cluster time series has a standard deviation of 2.2 cm compared to the 5 cm of the western Australian, South China Sea cluster.

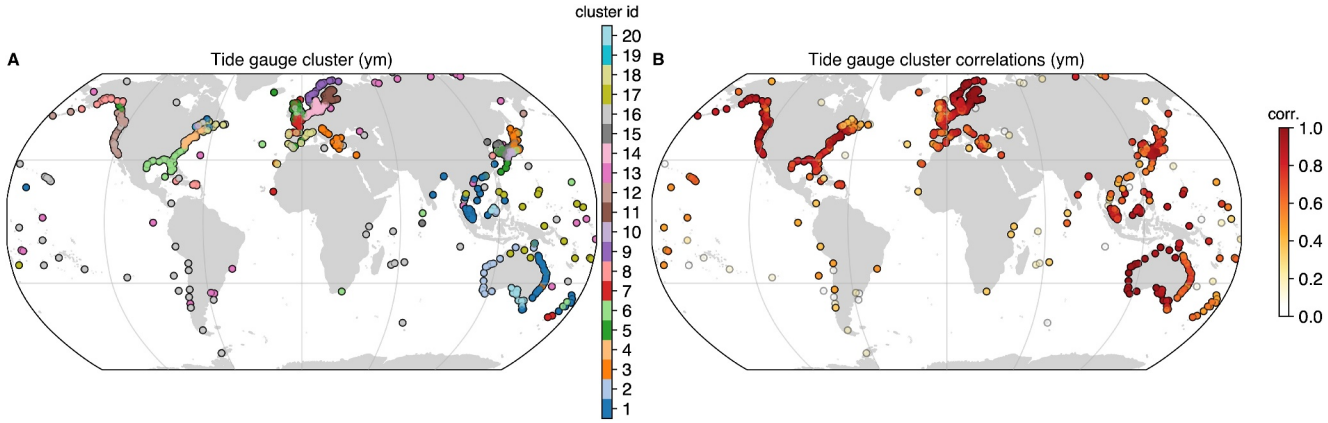

Figure 6. Clusters based annual (a) tide gauge observations. (b) Shows correlations of cluster time series $\mu_{t,k}$ with the associated monthly individual station time series. Points with correlations below 0.3 are shown as gray-outlined circles.

Since there are very few tide gauges along the coasts of Southeast and South Asia, Africa, and eastern South America, altimetry data can contribute to a better understanding of coastal sea level variations in these regions. However, even though some of the regions are associated with high coherence, many other regions, particularly the African and eastern South American and Australian coasts, cannot be associated with any detected coherent cluster (as expressed by the very low correlations with the altimetry clusters in Figure 2b). However, such poorly correlated locations can also be informative as they may indicate the dominance of local processes. For example, the altimetry-based cluster number five, which is shown in more detail in Figure S6 in Supporting Information S1, aggregates several globally distributed locations but has an overall very low average correlation of 0.2 with the virtual stations and an increased uncertainty of 1.3 cm (which is by a factor of 2 and 3 larger than the uncertainties of the nine most robust tide gauge cluster mean time series). Therefore, this cluster combines time series, which cannot be associated with any other nearby cluster. Interestingly, several of these locations are situated near river mouths, deltas, or freshwater lagoons, such as the Orinoco Delta, the Amazon Delta, the Ganges Delta, the Salween River, the Curonian Lagoon, or the semi-enclosed Salish Sea. Therefore, these poorly correlated clusters can reveal local effects, such as river runoff, that can cause a decrease in alongshore coherence and motivate further research to investigate these effects in more detail.

3.4. Timescale Dependency of Regional Pattern

Although several previous studies substantiated the separation of coherence at Cape Hatteras (Ezer, 2019; C. W. Hughes et al., 2018; Little et al., 2021; Piecuch et al., 2016), Little et al. (2021) emphasized that the spatial coherence in this region is strongly dependent on the time period considered as well as on the frequency itself. Therefore, to explore the sensitivity to the timescale, we repeat the Bayesian mixture model cluster estimation with annual tide gauge data.

Figures 2a and 6a reveal a high regional consistency of the cluster when derived from either monthly or annual averages. Similar regions are detected for most of the major tide gauge clusters, such as the NW-US Coast, the NE-US Coast, the NE-US and GOM, or the Baltic Sea. In some areas, such as Japan or Southeast Asia, we observe larger differences when comparing the results based on these different time scales, which might, however, be difficult to interpret due to the partially low number of stations in these regions.

We also investigate these cluster characteristics at longer timescales using correlations with the cluster time series based on 3-year-low-pass filtered data (applied to the monthly time series in Figure S2 in Supporting Information S1). As can be seen, at timescales longer than 3 years the separation between some clusters becomes less apparent. In particular, the clusters north and south of Cape Hatteras (here called NE-US Coast and NE-US + GOM) are more consistent at these longer timescales (i.e., more correlated), which is also supported by Little et al. (2021), who looked at 10–15 years band-pass filtered data. These results are consistent with the general expectation that the spatial scales of the ocean's response to atmospheric forcing will grow larger with a longer timescale (e.g., Philander, 1978). The higher consistency on longer timescales in the North Atlantic is also consistent with results from numerical simulations from C. W. Hughes et al. (2018), who showed that ocean

bottom pressure signals associated with the depth-independent (barotropic) mode (at timescales of 1.5–10 years) are highly uniform over the Atlantic continental shelves, which may explain some of the increased consistency of coastal sea level variations at such timescales.

At timescales longer than 3 years, we also find higher correlations between sea level along the Gulf of Mexico, the NW-US Coast, the eastern North Atlantic (i.e., the northern Europe cluster), and parts of the Mediterranean Sea, suggesting a common large-scale driver of these variations (Figure S2 in Supporting Information S1). These common variations could be caused by teleconnection mechanisms, such as remote influences of ENSO in particular on decadal NE-US Coast sea level variability as reported in previous work (Han et al., 2019; Valle-Levinson et al., 2017; Wise, Polton, et al., 2020).

Overall, these results emphasize that the clusters are largely consistent from monthly to annual timescales, whereas on longer (multiannual) timescales, the spatial scales of coherent coastal sea level variations increase in basins such as the North Atlantic. We also note that the increase in spatial scales could also be reflective of a reduction in the degrees of freedom relative to monthly time series.

3.5. Interdependencies Between Coastal Sea-Level Clusters and Climate Modes

In light of the extensive research in linking climate modes and sea level variability (e.g., Han et al., 2017, 2019; Royston et al., 2022; Stammer et al., 2013; J. Wang et al., 2021), an obvious question to ask is to what extent these clusters of coastal sea level variations are related to large-scale climate modes resulting from ocean-atmosphere interactions, and where they are more independent and unique to individual coastal regions. Our aim here is to examine these relationships from the perspective of the detected modes of coastal variability, which are independently estimated from the large-scale climate modes. By using coastal along-track altimetry data, we extend previous studies, which were based on model or gridded altimetry data (e.g., Han et al., 2019; Royston et al., 2022; J. Wang et al., 2021). Since we are considering the coastal cluster mean time series, we obtain additional insights into the relationships with climate modes at the regional scale since the clustering averages out some of the local variability at the individual stations. The ultimate goal of this investigation is to provide a basis for future analyses focusing on the pathways of atmospheric or oceanic forcing to coastal sea level variability.

In Figures 7a and 7b, we give an overview of the correlations between the monthly cluster time series (based on tide gauges and coastal altimetry) and a set of climate indices, NAO, EA, PNA, EA/WR, SCA, AO, ENSO, and the PDO (see also Section 2.2). We also show how much variance of the cluster time series $\mu_{k,t}$ is explained by a climate mode (c). We performed additional regression analyses considering the climate mode and its Hilbert transform (not shown), but the results were almost identical.

The highest correlations (and explained variances) with the cluster time series are found for the ENSO, PDO, and AO indices. As ENSO and PDO are themselves highly correlated (Han et al., 2019), they explain a similar amount of variability of different clusters in the Pacific and Indian Oceans (Figures 7c and 7d). ENSO is highly correlated with sea level along the eastern boundary of the Pacific (i.e., the NW-US cluster) and in antiphase with variations in the tropical Western Pacific (the East Indonesia cluster) as well as on the West coast of Australia (see also, e.g., Zhang & Church, 2012). These results are highly consistent with the current understanding of the mechanisms behind these connections. Several previous studies have consolidated that eastward propagating equatorial Kelvin waves associated with ENSO-related tropical wind forcing cause, upon impinging on a western boundary poleward coastally trapped signals that can explain large fractions of coastal sea level variability along the Pacific North and South American coasts (Clarke, 1992; Enfield & Allen, 1980; P. R. Thompson et al., 2014; J. Wang et al., 2021; Zhang & Church, 2012). In the western Pacific, it has been argued that sea level is driven by Rossby waves forced by variations in wind stress curl associated with ENSO and PDO (Han et al., 2019).

Slightly lower correlations with climate modes (e.g., with the NAO or the AO) are found for most of the marginal and semi-enclosed seas, such as for the Baltic Sea, the north European or the Mediterranean cluster (Figure 7b), which are mostly attributed to atmospheric wind stress and pressure forcing (Chafik et al., 2017; Dangendorf et al., 2014; Gomis et al., 2008; Jevrejeva et al., 2005; Passaro et al., 2021; J. Wang et al., 2021). There are differences in these correlations between the tide gauge and altimetry clusters due to the partially different distribution of the (virtual) stations (e.g., for the east Australian/Mediterranean and the Japanese clusters). For example, the Japanese cluster based on altimetry data includes more stations around the Sea of Japan and shows a significant correlation with ENSO, whereas the corresponding tide gauge cluster includes more stations on the

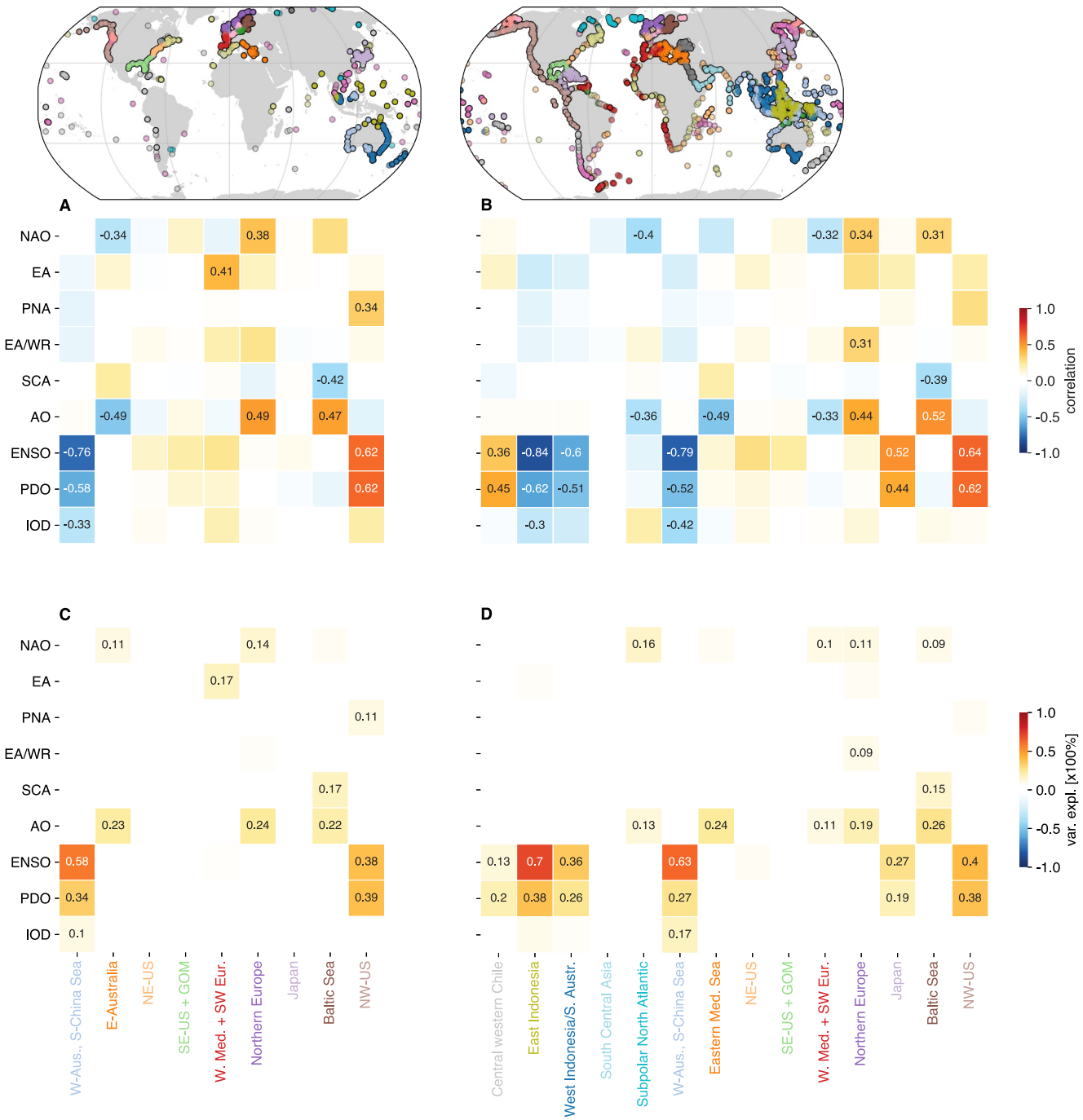

Figure 7. Correlations between monthly cluster time series and climate indices for the tide gauge data (a) and altimetry data (b). Only correlations with absolute values greater than 0.3 are represented by numbers. (c) and (d) Show the explained variance of the cluster time series by a climate index. Only fractions with absolute values greater than 0.3^2 are represented by numbers. The cluster maps at the top are the same as in Figures 4a and 4b.

east and south coasts of Japan and seems to be largely unrelated to ENSO. Thus, due to the limited number of stations, the tide gauge clusters sometimes aggregate stations where sea levels are not always fully physically connected, further supporting the importance of considering coastal altimetry data here as well.

Although we observe relatively high correlations with ENSO in some regions, which mathematically explains up to 71% of the east Indonesian cluster (Figure 7d), very little (<=38%) of the variance of the coastal sea level clusters can be mathematically explained by the remaining climate modes (Figure 7d). Thus, other drivers and

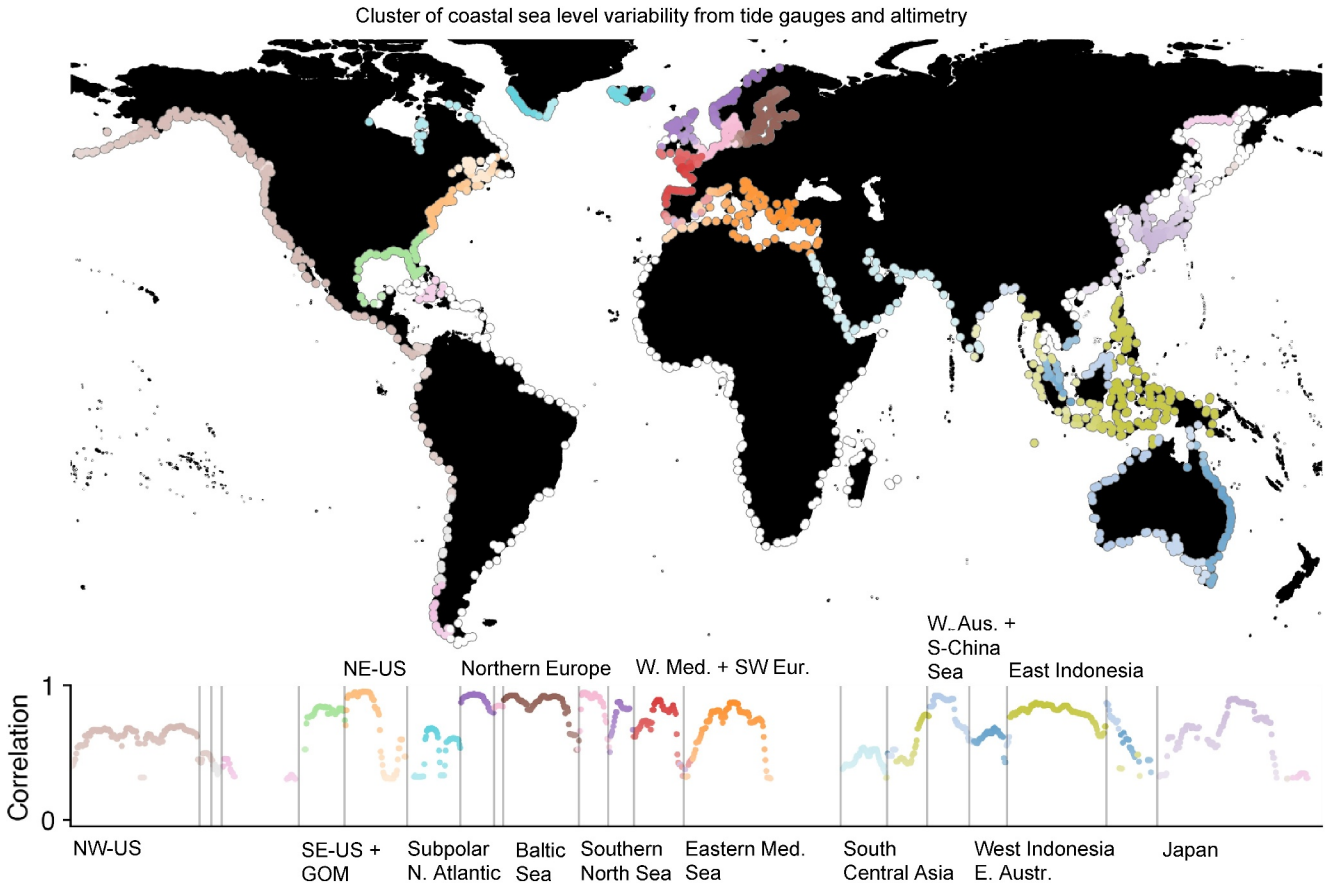

Figure 8. Summary of the clusters of coherent coastal sea level variations from tide gauges altimetry. Here, the colors indicate the cluster membership, whereas their opacity is inversely scaled by the correlation of the virtual station or tide gauge with the cluster mean time series. Shown are tide-gauge-based clusters for the NE-US coast, the SE-US coast and GOM, northern Europe, the southern North Sea, western Med. Sea and the southwestern European coastline, western Australia and the South China Sea, and Japan. We also show the west Indonesia and eastern Australia cluster, which is similar to the altimetry-based west Indonesia and southern Australia cluster. Altimetry-based clusters are shown for the NW-US coast, central western Chile, the subpolar North Atlantic, the Baltic Sea, the eastern Med. Sea, South Central Asia, and east Indonesia. At the bottom, we show the best correlations of each station with the cluster mean time series.

mechanisms must also be considered to fully understand the sources of these variations (K. R. Thompson, 1986). The same is true for many of the western boundary clusters, such as the northeast US coast, the Southeast American coast, or the eastern Australian coast. Here, the climate modes are poorly correlated with the cluster time series (Figures 7a and 7b).

Overall, the average of the maximum absolute correlations between each individual cluster time series and all climate indices considered is 0.41 for the tide gauge network and 0.47 for the altimetry data. This analysis supports the idea that a large fraction of coastal sea level variability manifests distinctly from the adjacent deep ocean, which could not be demonstrated in previous studies when limited to the geographically incomplete tide gauge database (e.g., Papadopoulos & Tsimplis, 2006). Although the literature has shown that large-scale patterns of coupled ocean-atmosphere variability directly drive much of the deep ocean sea level variability (Han et al., 2017, 2019; Stammer et al., 2013), our analysis suggests the situation is more complex at the coast. This is evident on monthly time scales from the medium-to-weak correlations between climate indices and a number of the clusters. As some of the detected coastal modes of variability are not simply a reflection of the climate modes, future efforts are required to identify their underlying drivers.

4. Conclusions

Here, we provide a systematic and quantitative analysis of the regions of coherent sea level variability on a global scale. Using a Bayesian mixture model, we cluster monthly coastal sea level variations from tide gauges and

coastal altimetry and identify regions where coastal sea level along the shelf is highly correlated. In doing so, we extend existing studies that have supported the existence of high regional coherence and thoroughly investigated the pattern of these variations but have mostly been limited to the well-instrumented areas around Europe and North America (Calafat et al., 2013, 2018; Enfield & Allen, 1980; Hermann et al., 2009; Hogarth et al., 2020; C. Hughes et al., 2019; Papadopoulos & Tsimplis, 2006).

We find that many of the coastal regions can indeed be clustered into regions of coherent coastal sea level variations using unsupervised learning and are largely robust across the different underlying measurement systems (tide gauges or coastal altimetry). In Figure 8, we summarize the most robust clusters from both data sets. Here, we select the tide-gauge-based clusters for the NE-US coast, the SE-US coast and GOM, northern Europe, the southern North Sea, the western Med. Sea, and the southwestern European coastline, western Australia and the South China Sea, and Japan. We also show the west Indonesia and eastern Australia cluster (based on tide gauges), which is similar to the altimetry-based west Indonesia and southern Australia cluster. Altimetry-based clusters are shown for the NW-US coast, central western Chile, the subpolar North Atlantic, the Baltic Sea, the eastern Med. Sea, South Central Asia, and east Indonesia. The nine most highly correlated clusters (for the tide gauge time series) have an average correlation of 0.82 at the monthly timescale and cover most European, North American, Australian, and Japanese tide gauges. This is a striking result, as it supports the hypothesis that much of the variability observed by tide gauges (in these regions) can be attributed to a set of common driving factors. Therefore, this disentangling of the regional clustering of variability represents a basis for future analyses focused on understanding the causes of these common variations.

The inclusion of coastal altimetry in our investigations reveals many more regions of coherent coastal sea level variations than can be observed by the tide gauge network alone (Figure 8). Many of these additionally detected station clusters, particularly in the Indian Ocean, have so far been poorly described or not described at all. Using the altimetry data, we also obtain a much better understanding of where the monthly sea level variations are highly coherent and where they are not. Although we find generally high correlations with the cluster time series at the eastern boundaries, marginal, and semi-enclosed seas, some stations along the western boundaries appear to be poorly captured by the cluster analysis (see also Figure 8). The causes of these characteristics need to be better understood, particularly for the eastern South American, African, and Australian coasts, where we do not find highly correlated cluster time series. In addition, although we find that the detected clusters are largely consistent at the monthly and annual timescales, we observe enhanced coherency within and across the ocean basins (e.g., the Atlantic and Eastern Pacific) at longer timescales. Therefore, mechanistic explanations of the drivers of the coastal clusters should take this dependence on the timescale into account.

We investigate the role of climate modes in shaping coastal sea level variations at the monthly timescale. We consider these relationships using a global coastal altimetry product and use the cluster mean time series to reduce some of the local variability at individual stations. A significant proportion of the clusters, that is, at the eastern boundary of the Pacific, the Western tropical Pacific, and the marginal and semi-enclosed seas, are correlated with climate modes such as ENSO, NAO, or AO, which is highly consistent with widely accepted knowledge (Chafik et al., 2017; Clarke, 1992; Dangendorf et al., 2014; Enfield & Allen, 1980; Gomis et al., 2008; Han et al., 2017, 2019; Jevrejeva et al., 2005; Passaro et al., 2021; P. R. Thompson et al., 2014; Zhang & Church, 2012; J. Wang et al., 2021). The transmission of equatorial forcing (linked to ENSO) along the eastern boundaries appears to contribute to the high coherence in some of these regions.

However, and more importantly, the results also show that several other clusters, especially along the western boundaries, share very little variability with the considered climate modes. At a global level, the correlation between cluster time series and the best-correlated climate index for each cluster averages only 0.39. Despite the partially missing or weak links to large-scale climate modes, coastal sea level variations often appear to exhibit highly coherent behavior (e.g., the NE-US coastal cluster, the south-central Asian cluster, or the southwestern European cluster). These results confirm that, although large-scale climate modes explain much of the global spatial sea level variability, many coastal zones exhibit variations whose dynamics are different from variability associated with climate modes. Therefore, the identified clusters of coastal variability provide an important basis for future work aimed at better understanding the drivers and pathways of open ocean or atmospheric forcing on coastal sea level variability, which in most cases are not directly related to large-scale climate modes at monthly timescales but have different common origins.

4.1. Discussion of the Causes of Coastal Coherence and De-Coupling of Coastal and Open Ocean Variability

Our investigations leave many unanswered questions that need to be better understood and resolved in future work. In particular, this concerns the causes of the differences in coherence between different coastal regions and of the decoupling of coastal and open ocean variability. In general, coastal and open ocean sea level can differ because of three reasons (Williams & Hughes, 2012). First, sea level variability in shallow waters can be dominated by local forcing, such as wind stress or atmospheric pressure. This local forcing is mostly reflected by the enhanced high-frequency content in the spectra of sea level variability especially in areas with wider shelves or semi-enclosed seas (C. W. Hughes & Williams, 2010). In addition to atmospheric forcing, river discharge can also cause large differences between coastal and open ocean sea level variability. Using models and observations (Piecuch, 2023; Piecuch & Wadehra, 2020; Piecuch et al., 2018) showed that river discharge has a significant effect on local and regional sea level on monthly, seasonal, and interannual up to centennial timescales in the Río de la Plata estuary. Understanding these effects on coastal sea level may, therefore, help to interpret some of the regional differences in the clusters detected.

The second cause of differences between coastal and open ocean sea level variability is the role of bathymetry, which can isolate coastal waters from deep ocean signals. Although deep ocean sea level is primarily driven by steric changes, being a depth-integrated signal, the contribution of the steric signal decreases toward the coast. Therefore, a large fraction of coastal sea level variability is due to mass changes and thus reflected in a bottom pressure signal (Dangendorf et al., 2021; C. W. Hughes et al., 2018; Steinberg et al., 2024). In contrast to small islands, where the effect of topography is minimal, Williams and Hughes (2012) and C. W. Hughes et al. (2018) showed that the topography of the continental shelves acts as a barrier to mesoscale variability. The suppression of this deep ocean signal depends on several factors, such as the Rossby number, bottom slope, and eddy scale. For example, Wise et al. (2018) and Wise, Hughes, et al. (2020) used an idealized model to show that the width and steepness of the continental shelf and slope affect the extent to which deep ocean variability can penetrate the coast by modifying the effective bottom friction. This implies that regions, where the coast is very far from the deep ocean are relatively more insulated from deep ocean variability, and consequently, on-shelf processes exert an even stronger influence on coastal sea level coherence in these regions. Thus, regions such as the NE-US coastal shelf or the Argentine shelf may be less sensitive to forcing from the ocean interior and more dominated by on-shelf processes and local wind forcing than regions with narrower shelves (e.g., the coasts of Australia or Africa).

Finally, the third factor that causes differences between coastal and open ocean variability is the difference in the processes that dominate these different regimes. For example, these differences are particularly pronounced at western boundaries, where deep ocean sea level is dominated by high-frequency mesoscale variability. On the other hand, processes that are unique to the coast, such as coastally trapped waves, not only cause differences between coastal and open ocean sea level variability but also contribute to the alongshore coherence of coastal sea level variability (C. W. Hughes et al., 2018). However, regional model-based investigations are required to disentangle the complex interplay of local and remote forcing, the cross-shelf transport and the role of coastally trapped waves to establish these coherent variations. As an example, Wise et al. (2024) used an ocean model to understand the different contributions to sea level on the northwest European Shelf. They found that—as suggested by earlier studies (Calafat et al., 2012)—that coastal trapped waves are associated with sea level variations on the western northwest European Shelf, which can explain the coherent cluster identified in this region.

Although these factors need to be clarified, another challenge is the potential spatiotemporal nonstationarity of the coherent regions, which is difficult to detect for this relatively short time period. If some of the forcing factors, such as slow changes in the ocean circulation or the climate modes themselves, exhibit nonstationary variations, we may not be able to fully comprehend their effects on the modes of coastal variability beyond the period considered here. In fact, based on wavelet analysis, Little et al. (2021) reported different regimes in the variability of the NE-US coastal sea level with a spectral peak in the power spectrum at a period of about 12.4 years between 1950 and 2000 and much lower decadal variability after 2000. Such effects may therefore be hidden from our analysis and could be further investigated in future work. Since we have focused primarily on the monthly timescale, we need to determine the frequency-dependent effects of climate modes on the coastal modes. Finally, as the comparison of climate modes and sea level on a monthly timescale can only provide general hypotheses about the underlying drivers, further investigations are required to understand the coupling/decoupling of the

coastal modes and open ocean variability and the implications of these relationships for long-term coastal sea level trends.

Knowledge of the detected coherent regions represents a starting point for more extensive future investigations. This includes analyses of how the coastal sea level variations are captured in sea level reconstructions (Dangendorf et al., 2019) and how well they can represent open ocean changes, as sea level reconstructions are commonly constrained by EOFs from sea level data associated with large-scale climate variability (from global data). Closely related to this point is the question of how coastal sea level variability will change in the future. This could be better understood if we identify the common drivers of the coherent modes of variability, and how they are projected to respond to future climate changes. Our analyses also motivate to focus on regions that have not yet been sufficiently studied, which is now possible with coastal altimetry.

Data Availability Statement

Monthly tide gauge data from PSMSL are available at https://www.psmsl.org/data/obtaining/ (Holgate et al., 2013). We use dedicated coastal 1-Hz along-track altimetry data of the missions Jason 1–Jason 3 from DGFI-TUM's OpenADB (Schwatke et al., 2023). Gridded altimetry (Global Ocean Gridded L 4 Sea Surface Heights And Derived Variables Reprocessed 1993 Ongoing (Dataset), n.d.) data is available at https://resources.marine.copernicus.eu/product-detail/SEALEVEL_GLO_PHY_L4_MY_008_047/INFORMATION. The estimated cluster properties for the tide gauge and the coastal altimetry data can be found here Oelsmann et al. (2024).

Acknowledgments
This research was supported by the International Space Science Institute (ISSI) in Bern through ISSI International Team project 524. C.G.P was supported by the NASA Sea Level Change Team (Grant 80NSSC20K1241), GRACE Follow-On Science Team (Grant 80NSSC20K0728), and Ocean Surface Topography Science Team (JPL subcontract 1670515). A.W. was funded by the NERC CANARI project (NE/W004984/1). S.J was supported by NERC NC International programme: Future states of the global Coastal ocean: Understanding for Solutions (FOCUS: NE/X006271/1) and NC AtlatniS funding (NE/Y005589/1). We thank Carolina Camargo and Sönke Dangendorf for their helpful comments. Open Access funding enabled and organized by Projekt DEAL.

References

Altamimi, Z., Rebischung, P., Métivier, L., & Collilieux, X. (2016). Journal of geophysical research: Solid Earth ITRF2014: A new release of the international terrestrial reference frame modeling nonlinear station motions. *Journal of Geophysical Research: Solid Earth*, *121*(8), 6109–6131. https://doi.org/10.1002/2016JB013098

Andersen, O. B., Nielsen, K., Knudsen, P., Hughes, C. W., Fenoglio-marc, L., Gravelle, M., & Polo, S. P. (2018). Improving the coastal mean dynamic topography by geodetic combination of tide gauge and satellite altimetry improving the coastal mean dynamic topography by geodetic combination of tide gauge and satellite altimetry. *Marine Geodesy*, *0*(0), 1–29. https://doi.org/10.1080/01490419.2018.1530320

Andres, M., Gawarkiewicz, G. G., & Toole, J. M. (2013). Interannual sea level variability in the western north Atlantic: Regional forcing and remote response. *Geophysical Research Letters*, *40*(22), 5915–5919. https://doi.org/10.1002/2013GL058013

Bosch, W., Dettmering, D., & Schwatke, C. (2014). Multi-mission cross-calibration of satellite altimeters: Constructing a long-term data record for global and regional sea level change studies. *Remote Sensing*, *6*(3), 2255–2281. https://doi.org/10.3390/rs6032255

Bosch, W., & Savcenko, R. (2007). *Satellite altimetry: Multi-mission cross calibration*. International association of geodesy symposia. https://doi.org/10.1007/978-3-540-49350-1_8

Calafat, F. M., Chambers, D. P., & Tsimplis, M. N. (2012). Mechanisms of decadal sea level variability in the eastern north Atlantic and the Mediterranean Sea. *Journal of Geophysical Research*, *117*(C9). https://doi.org/10.1029/2012JC008285

Calafat, F. M., Chambers, D. P., & Tsimplis, M. N. (2013). Inter-annual to decadal sea-level variability in the coastal zones of the Norwegian and Siberian Seas: The role of atmospheric forcing. *Journal of Geophysical Research: Oceans*, *118*(3), 1287–1301. https://doi.org/10.1002/jgrc.20106

Calafat, F. M., Wahl, T., Lindsten, F., Williams, J., & Frajka-Williams, E. (2018). Coherent modulation of the sea-level annual cycle in the United States by Atlantic Rossby waves. *Nature Communications*, *9*(1), 2571. https://doi.org/10.1038/s41467-018-04898-y

Camargo, C. M. L., Riva, R. E. M., Hermans, T. H. J., Schütt, E. M., Marcos, M., Hernandez-Carrasco, I., & Slangen, A. B. A. (2023). Regionalizing the sea-level budget with machine learning techniques. *Ocean Science*, *19*(1), 17–41. https://doi.org/10.5194/os-19-17-2023

Carrère, L., Faugère, Y., & Ablain, M. (2016). Major improvement of altimetry sea level estimations using pressure-derived corrections based on era-interim atmospheric reanalysis. *Ocean Science*, *12*(3), 825–842. https://doi.org/10.5194/os-12-825-2016

Carrère, L., & Lyard, F. (2003). Modeling the barotropic response of the global ocean to atmospheric wind and pressure forcing—Comparisons with observations. *Geophysical Research Letters*, *30*(6). https://doi.org/10.1029/2002GL016473

Carrère, L., Lyard, F., Cancet, M., & Guillot, A. (2015). FES 2014, a new tidal model on the global ocean with enhanced accuracy in shallow seas and in the Arctic region. In *EGU General Assembly Conference Abstracts* (p. 5481).

Cazenave, A., Gouzenes, Y., Birol, F., Leger, F., Passaro, M., Calafat, F. M., et al. (2022). Sea level along the world's coastlines can be measured by a network of virtual altimetry stations. *Communications Earth & Environment*, *3*(1), 117. https://doi.org/10.1038/s43247-022-00448-z

Chafik, L., Nilsen, J. E. I., & Dangendorf, S. (2017). Impact of north Atlantic teleconnection patterns on northern European Sea level. *Journal of Marine Science and Engineering*, *5*(3), 43. https://doi.org/10.3390/jmse5030043

Chafik, L., Nilsen, J. E. Ø., Dangendorf, S., Reverdin, G., & Frederikse, T. (2019). North Atlantic Ocean circulation and decadal sea level change during the altimetry era. *Scientific Reports*, *9*(1), 1041. https://doi.org/10.1038/s41598-018-37603-6

Church, J., & White, N. (2011). Sea-level rise from the late 19th to the early 21st century. *Surveys in Geophysics*, *32*(4–5), 585–602. https://doi.org/10.1007/s10712-011-9119-1

Clarke, A. J. (1992). Low-frequency reflection from a nonmeridional eastern ocean boundary and the use of coastal sea level to monitor eastern pacific equatorial kelvin waves. *Journal of Physical Oceanography*, *22*(2), 163–183. https://doi.org/10.1175/1520-0485(1992)022⟨0163:LFRFAN⟩2.0.CO;2

Dangendorf, S., Calafat, F. M., Arns, A., Wahl, T., Haigh, I. D., & Jensen, J. (2014). Mean sea level variability in the north sea: Processes and implications. *Journal of Geophysical Research: Oceans*, *119*(10). https://doi.org/10.1002/2014JC009901

Dangendorf, S., Frederikse, T., Chafik, L., Klinck, J. M., Ezer, T., & Hamlington, B. D. (2021). Data-driven reconstruction reveals large-scale ocean circulation control on coastal sea level. *Nature Climate Change*, *11*(6), 514–520. https://doi.org/10.1038/s41558-021-01046-1

Dangendorf, S., Hay, C., Calafat, F. M., Marcos, M., Piecuch, C. G., Berk, K., & Jensen, J. (2019). Persistent acceleration in global sea-level rise since the 1960s. *Nature Climate Change*, *9*(9), 705–710. https://doi.org/10.1038/s41558-019-0531-8

Enfield, D. B., & Allen, J. S. (1980). On the structure and dynamics of monthly mean sea level anomalies along the Pacific coast of north and south America. *Journal of Physical Oceanography*, *10*(4), 557–578. https://doi.org/10.1175/1520-0485(1980)010⟨0557:OTSADO⟩2.0.CO;2

Ezer, T. (2019). Regional differences in sea level rise between the mid-Atlantic bight and the south Atlantic bight: Is the gulf stream to blame? *Earth's Future*, *7*(7), 771–783. https://doi.org/10.1029/2019EF001174

Fernandes, M. J., & Lázaro, C. (2016). GPD+ wet tropospheric corrections for CryoSat-2 and GFO altimetry missions. *Remote Sensing*, *8*(10), 851. https://doi.org/10.3390/rs8100851

Frederikse, T., Landerer, F., Caron, L., Adhikari, S., Parkes, D., Humphrey, V. W., et al. (2020). The causes of sea-level rise since 1900. *Nature*, *584*(7821), 393–397. https://doi.org/10.1038/s41586-020-2591-3

Frederikse, T., Landerer, F. W., & Caron, L. (2019). The imprints of contemporary mass redistribution on local sea level and vertical land motion observations. *Solid Earth*, *10*(6), 1971–1987. https://doi.org/10.5194/se-10-1971-2019

Frederikse, T., Riva, R., Kleinherenbrink, M., Wada, Y., van den Broeke, M., & Marzeion, B. (2016). Closing the sea level budget on a regional scale: Trends and variability on the northwestern European continental shelf. *Geophysical Research Letters*, *43*(20), 10864–10872. https://doi.org/10.1002/2016GL070750

Frederikse, T., Riva, R., Slobbe, C., Broerse, T., & Verlaan, M. (2016). Estimating decadal variability in sea level from tide gauge records: An application to the north sea. *Journal of Geophysical Research: Oceans*, *121*(3), 1529–1545. https://doi.org/10.1002/2015JC011174

Frederikse, T., Simon, K., Katsman, C. A., & Riva, R. (2017). The sea-level budget along the northwest Atlantic coast: Gia, mass changes, and large-scale ocean dynamics. *Journal of Geophysical Research: Oceans*, *122*(7), 5486–5501. https://doi.org/10.1002/2017JC012699

Global ocean gridded l 4 sea surface heights and derived variables reprocessed 1993 ongoing. (n.d.). Global ocean gridded l 4 sea surface heights and derived variables reprocessed 1993 ongoing [Dataset]. https://doi.org/10.48670/moi-00148

Gomis, D., Ruiz, S., Sotillo, M. G., Álvarez Fanjul, E., & Terradas, J. (2008). Low frequency Mediterranean Sea level variability: The contribution of atmospheric pressure and wind. *Global and Planetary Change*, *63*(2), 215–229. https://doi.org/10.1016/j.gloplacha.2008.06.005

Gräwe, U., Klingbeil, K., Kelln, J., & Dangendorf, S. (2019). Decomposing mean sea level rise in a semi-enclosed basin, the Baltic Sea. *Journal of Climate*, *32*(11), 3089–3108. https://doi.org/10.1175/JCLI-D-18-0174.1

Gregory, J. M., Griffies, S. M., Hughes, C. W., Lowe, J. A., Church, J. A., Fukimori, I., & Tamisiea, M. E. (2019). In *Concepts and Terminology for Sea Level: Mean, Variability and Change, Both Local and Global* (Vol. 0123456789). https://doi.org/10.1007/s10712-019-09525-z

Han, W., Meehl, G. A., Stammer, D., Hu, A., Hamlington, B., Kenigson, J., et al. (2017). Spatial patterns of sea level variability associated with natural internal climate modes. *Surveys in Geophysics*, *38*(1), 217–250. https://doi.org/10.1007/s10712-016-9386-y

Han, W., Stammer, D., Thompson, P., Ezer, T., Palanisamy, H., Zhang, X., et al. (2019). Impacts of basin-scale climate modes on coastal sea level: A review. *Surveys in Geophysics*, *40*(6), 1493–1541. https://doi.org/10.1007/s10712-019-09562-8

Hardman-Mountford, N., Richardson, A., Boyer, D., Kreiner, A., & Boyer, H. (2003). Relating sardine recruitment in the northern benguela to satellite-derived sea surface height using a neural network pattern recognition approach. *Progress in Oceanography*, *59*(2), 241–255. (ENVIFISH: Investigating environmental causes of pelagic fisheries variability in the SE Atlantic). https://doi.org/10.1016/j.pocean.2003.07.005

Hay, C. C., Morrow, E., Kopp, R. E., & Mitrovica, J. X. (2015). Probabilistic reanalysis of twentieth-century sea-level rise. *Nature*, *517*(7535), 481–484. https://doi.org/10.1038/nature14093

Hermann, A. J., Curchitser, E. N., Haidvogel, D. B., & Dobbins, E. L. (2009). A comparison of remote vs. local influence of El Niño on the coastal circulation of the northeast Pacific. *Deep Sea Research Part II: Topical Studies in Oceanography*, *56*(24), 2427–2443. https://doi.org/10.1016/j.dsr2.2009.02.005

Hermans, T. H. J., Le Bars, D., Katsman, C. A., Camargo, C. M. L., Gerkema, T., Calafat, F. M., et al. (2020). Drivers of interannual sea level variability on the northwestern European shelf. *Journal of Geophysical Research: Oceans*, *125*(10), e2020JC016325. https://doi.org/10.1029/2020JC016325

Hogarth, P., Hughes, C., Williams, S., & Wilson, C. (2020). Improved and extended tide gauge records for the British Isles leading to more consistent estimates of sea level rise and acceleration since 1958. *Progress in Oceanography*, *184*, 102333. https://doi.org/10.1016/j.pocean.2020.102333

Holgate, S. J., Matthews, A., Woodworth, P. L., Rickards, L. J., Tamisiea, M. E., Bradshaw, E., et al. (2013). New data systems and products at the permanent service for mean sea level [Dataset]. *Journal of Coastal Research*, 493–504. https://doi.org/10.2112/JCOASTRES-D-12-00175.1

Hughes, C., Fukumori, I., Griffies, S. M., Huthnance, J. M., Minobe, S., Spence, P., et al. (2019). Sea level and the role of coastal trapped waves in mediating the influence of the open ocean on the coast. *Surveys in Geophysics*, *40*(6), 1467–1492. https://doi.org/10.1007/s10712-019-09535-x

Hughes, C., & Meredith, M. (2006). Coherent sea-level fluctuations along the global continental slope. *Philosophical Transactions. Series A, Mathematical, Physical, and Engineering Sciences*, *364*(1841), 885–901. https://doi.org/10.1098/rsta.2006.1744

Hughes, C. W., Williams, J., Blaker, A., Coward, A., & Stepanov, V. (2018). A window on the deep ocean: The special value of ocean bottom pressure for monitoring the large-scale, deep-ocean circulation. *Progress in Oceanography*, *161*, 19–46. https://doi.org/10.1016/j.pocean.2018.01.011

Hughes, C. W., & Williams, S. D. P. (2010). The color of sea level: Importance of spatial variations in spectral shape for assessing the significance of trends. *Journal of Geophysical Research*, *115*(C10). https://doi.org/10.1029/2010JC006102

Hünicke, B., & Zorita, E. (2006). Influence of temperature and precipitation on decadal Baltic Sea level variations in the 20th century. *Tellus A: Dynamic Meteorology and Oceanography*, *58*(1), 141–153. https://doi.org/10.1111/j.1600-0870.2006.00157.x

Intergovernmental Panel on Climate Change (IPCC). (2023). Ocean, cryosphere and sea level change. In *Climate change 2021 – The physical science basis: Working Group I contribution to the sixth assessment report of the Intergovernmental Panel on Climate Change* (pp. 1211–1362). Cambridge University Press.

Jevrejeva, S., Grinsted, A., Moore, J. C., & Holgate, S. (2006). Nonlinear trends and multiyear cycles in sea level records. *Journal of Geophysical Research*, *111*(C9). https://doi.org/10.1029/2005JC003229

Jevrejeva, S., Moore, J., Woodworth, P., & Grinsted, A. (2005). Influence of large-scale atmospheric circulation on European Sea level: Results based on the wavelet transform method. *Tellus*, *57*(2), 183. https://doi.org/10.3402/tellusa.v57i2.14609

Kalnay, E., Kanamitsu, M., Kistler, R., Collins, W., Deaven, D., Gandin, L., et al. (1996). The NCEP/NCAR 40-year reanalysis project. *Bulletin of the American Meteorological Society*, *77*(3), 437–472. https://doi.org/10.1175/1520-0477(1996)077⟨0437:TNYRP⟩2.0.CO;2

Landskron, D., & Böhm, J. (2018a). Refined discrete and empirical horizontal gradients in VLBI analysis. *Journal of Geodesy*, *92*(12), 1387–1399. https://doi.org/10.1007/s00190-018-1127-1

Landskron, D., & Böhm, J. (2018b). VMF3/GPT3: Refined discrete and empirical troposphere mapping functions. *Journal of Geodesy*, *92*(4), 349–360. https://doi.org/10.1007/s00190-017-1066-2

Little, C. M., Piecuch, C. G., & Ponte, R. M. (2021). North American east coast sea level exhibits high power and spatiotemporal complexity on decadal timescales. *Geophysical Research Letters*, *48*(15), e2021GL093675. https://doi.org/10.1029/2021GL093675
Liu, Y., Weisberg, R. H., Vignudelli, S., & Mitchum, G. T. (2016). Patterns of the loop current system and regions of sea surface height variability in the eastern gulf of Mexico revealed by the self-organizing maps. *Journal of Geophysical Research: Oceans*, *121*(4), 2347–2366. https://doi.org/10.1002/2015JC011493
Mclachlan, G., & Basford, K. (1988). In *Mixture models: Inference and applications to clustering* (Vol. 38). https://doi.org/10.2307/2348072
McLachlan, G. J., & Peel, D. (2000). *Finite mixture models*. Wiley Series in Probability and Statistics.
Oelsmann, J., Calafat, F., Wise, A., Katsman, C., Passaro, M., Dettmering, D., et al. (2024). Data supplement to "coherent modes of global coastal sea level variability". *Zenodo*. https://doi.org/10.5281/zenodo.14175287
Oelsmann, J., Passaro, M., Dettmering, D., Schwatke, C., Sánchez, L., & Seitz, F. (2021). The zone of influence: Matching sea level variability from coastal altimetry and tide gauges for vertical land motion estimation. *Ocean Science*, *17*(1), 35–57. https://doi.org/10.5194/os-17-35-2021
Papadopoulos, A., & Tsimplis, M. N. (2006). Coherent coastal sea-level variability at interdecadal and interannual scales from tide gauges. *Journal of Coastal Research*, *2006*(223), 625–639. https://doi.org/10.2112/04-0156.1
Passaro, M., Cipollini, P., Vignudelli, S., Quartly, G. D., & Snaith, H. M. (2014). ALES: A multi-mission adaptive subwaveform retracker for coastal and open ocean altimetry. *Remote Sensing of Environment*, *145*, 173–189. https://doi.org/10.1016/j.rse.2014.02.008
Passaro, M., Müller, F. L., Oelsmann, J., Rautiainen, L., Dettmering, D., Hart-Davis, M. G., et al. (2021). Absolute Baltic Sea level trends in the satellite altimetry era: A revisit. *Frontiers in Marine Science*, *8*. https://doi.org/10.3389/fmars.2021.647607
Passaro, M., Nadzir, Z. A., & Quartly, G. D. (2018). Improving the precision of sea level data from satellite altimetry with high-frequency and regional sea state bias corrections. *Remote Sensing of Environment*, *218*, 245–254. https://doi.org/10.1016/j.rse.2018.09.007
Petit, G., & Luzum, B. (2010). IERS conventions. In *Verlag des Bundesamts für Kartographie und Geodäsie*.
Phan, D., Pradhan, N., & Jankowiak, M. (2019). Composable effects for flexible and accelerated probabilistic programming in NumPyro.
Philander, S. G. H. (1978). Forced oceanic waves. *Reviews of Geophysics*, *16*(1), 15–46. https://doi.org/10.1029/RG016i001p00015
Piecuch, C. G. (2023). River effects on sea-level rise in the Río de la Plata estuary during the past century. *Ocean Science*, *19*(1), 57–75. https://doi.org/10.5194/os-19-57-2023
Piecuch, C. G., Bittermann, K., Kemp, A. C., Ponte, R. M., Little, C. M., Engelhart, S. E., & Lentz, S. J. (2018). River-discharge effects on United States Atlantic and gulf coast sea-level changes. *Proceedings of the National Academy of Sciences of the United States of America*, *115*(30), 7729–7734. https://doi.org/10.1073/pnas.1805428115
Piecuch, C. G., Dangendorf, S., Ponte, R. M., & Marcos, M. (2016). Annual sea level changes on the north American northeast coast: Influence of local winds and barotropic motions. *Journal of Climate*, *29*(13), 4801–4816. https://doi.org/10.1175/JCLI-D-16-0048.1
Piecuch, C. G., Fukumori, I., & Ponte, R. M. (2021). Intraseasonal sea level variability in the Persian gulf. *Journal of Physical Oceanography*, *51*(5), 1687–1704. https://doi.org/10.1175/JPO-D-20-0296.1
Piecuch, C. G., & Wadehra, R. (2020). Dynamic sea level variability due to seasonal river discharge: A preliminary global ocean model study. *Geophysical Research Letters*, *47*(4), e2020GL086984. https://doi.org/10.1029/2020GL086984
Rashid, M. M., Wahl, T., Chambers, D. P., Calafat, F. M., & Sweet, W. V. (2019). An extreme sea level indicator for the contiguous United States coastline. *Scientific Data*, *6*(1), 326. https://doi.org/10.1038/s41597-019-0333-x
Royston, S., Bingham, R. J., & Bamber, J. L. (2022). Attributing decadal climate variability in coastal sea-level trends. *Ocean Science*, *18*(4), 1093–1107. https://doi.org/10.5194/os-18-1093-2022
Scharroo, R., & Smith, W. H. F. (2010). A global positioning system–based climatology for the total electron content in the ionosphere. *Journal of Geophysical Research*, *115*(A10). https://doi.org/10.1029/2009JA014719
Schwatke, C., Dettmering, D., Passaro, M., Hart-Davis, M., Scherer, D., Müller, F. L., et al. (2023). Openadb: Dgfi-tum's open altimeter database. *Geoscience Data Journal*. https://doi.org/10.1002/gdj3.233
Stammer, D., Cazenave, A., Ponte, R. M., & Tamisiea, M. E. (2013). Causes for contemporary regional sea level changes. *Annual Review of Marine Science*, *5*(1), 21–46. (PMID: 22809188). https://doi.org/10.1146/annurev-marine-121211-172406
Steinberg, J. M., Piecuch, C. G., Hamlington, B. D., Thompson, P. R., & Coats, S. (2024). Influence of deep-ocean warming on coastal sea-level decadal trends in the gulf of Mexico. *Journal of Geophysical Research: Oceans*, *129*(1), e2023JC019681. https://doi.org/10.1029/2023JC019681
Thompson, K. R. (1986). North Atlantic sea-level and circulation. *Geophysical Journal International*, *87*(1), 15–32. https://doi.org/10.1111/j.1365-246X.1986.tb04543.x
Thompson, P. R., & Merrifield, M. A. (2014). A unique asymmetry in the pattern of recent sea level change. *Geophysical Research Letters*, *41*(21), 7675–7683. https://doi.org/10.1002/2014GL061263
Thompson, P. R., Merrifield, M. A., Wells, J. R., & Chang, C. M. (2014). Wind-driven coastal sea level variability in the northeast pacific. *Journal of Climate*, *27*(12), 4733–4751. https://doi.org/10.1175/JCLI-D-13-00225.1
Thompson, P. R., & Mitchum, G. T. (2014). Coherent sea level variability on the north Atlantic western boundary. *Journal of Geophysical Research: Oceans*, *119*(9), 5676–5689. https://doi.org/10.1002/2014JC009999
Thorndike, R. L. (1953). Who belongs in the family? *Psychometrika*, *18*(4), 267–276. https://doi.org/10.1007/BF02289263
Valle-Levinson, A., Dutton, A., & Martin, J. B. (2017). Spatial and temporal variability of sea level rise hot spots over the eastern United States. *Geophysical Research Letters*, *44*(15), 7876–7882. https://doi.org/10.1002/2017GL073926
Wang, J., Church, J. A., Zhang, X., & Chen, X. (2021). Reconciling global mean and regional sea level change in projections and observations. *Nature Communications*, *12*(1), 990. https://doi.org/10.1038/s41467-021-21265-6
Wang, O., Lee, T., Piecuch, C. G., Fukumori, I., Fenty, I., Frederikse, T., et al. (2022). Local and remote forcing of interannual sea-level variability at Nantucket Island. *Journal of Geophysical Research: Oceans*, *127*(6), e2021JC018275. https://doi.org/10.1029/2021JC018275
Williams, J., & Hughes, C. (2012). The coherence of small island sea level with the wider ocean: A model study. *Ocean Science Discussions*, *9*, 3049–3070. https://doi.org/10.5194/osd-9-3049-2012
Wise, A., Calafat, F. M., Hughes, C. W., Jevrejeva, S., Katsman, C. A., Oelsmann, J., et al. (2024). Using shelf-edge transport composition and sensitivity experiments to understand processes driving sea level on the northwest European shelf. *Journal of Geophysical Research: Oceans*, *129*(5), e2023JC020587. https://doi.org/10.1029/2023JC020587
Wise, A., Hughes, C. W., & Polton, J. (2018). Bathymetric influence on the coastal sea level response to ocean gyres at western boundaries. *Journal of Physical Oceanography*, *48*(12), 2949–2964. https://doi.org/10.1175/jpo-d-18-0007.1
Wise, A., Hughes, C. W., Polton, J. A., & Huthnance, J. M. (2020). Leaky slope waves and sea level: Unusual consequences of the beta effect along western boundaries with bottom topography and dissipation. *Journal of Physical Oceanography*, *50*(1), 217–237. https://doi.org/10.1175/JPO-D-19-0084.1

Wise, A., Polton, J. A., Hughes, C. W., & Huthnance, J. M. (2020). Idealised modelling of offshore-forced sea level hot spots and boundary waves along the north American east coast. *Ocean Modelling*, *155*, 101706. https://doi.org/10.1016/j.ocemod.2020.101706

Woodworth, P. L., Melet, A., Marcos, M., Ray, R. D., Wöppelmann, G., Sasaki, Y. N., et al. (2019). Forcing factors affecting sea level changes at the coast. *Surveys in Geophysics*, *40*(6), 1351–1397. https://doi.org/10.1007/s10712-019-09531-1

Zhang, X., & Church, J. A. (2012). Sea level trends, interannual and decadal variability in the Pacific Ocean. *Geophysical Research Letters*, *39*(21). https://doi.org/10.1029/2012GL053240